A Section 508–conformant HTML version of this article is available at https://doi.org/10.1289/EHP2589.

Comprehensive Analyses and Prioritization of Tox21 10K Chemicals Affecting Mitochondrial Function by in-Depth Mechanistic Studies

Menghang Xia,[1] Ruili Huang,[1] Qiang Shi,[2] Windy A. Boyd,[3] Jinghua Zhao,[1] Nuo Sun,[4] Julie R. Rice,[3] Paul E. Dunlap,[3] Amber J. Hackstadt,[5] Matt F. Bridge,[5] Marjolein V. Smith,[5] Sheng Dai,[1] Wei Zheng,[1] Pei-Hsuan Chu,[1] David Gerhold,[1] Kristine L. Witt,[3] Michael DeVito,[3] Jonathan H. Freedman,[6] Christopher P. Austin,[1] Keith A. Houck,[7] Russell S. Thomas,[7] Richard S. Paules,[3] Raymond R. Tice,[3] and Anton Simeonov[1]

[1]National Center for Advancing Translational Sciences, National Institutes of Health (NIH), Department of Health and Human Services (DHHS), Bethesda, Maryland, USA
[2]Division of Systems Biology, National Center for Toxicological Research, U. S. Food and Drug Administration, Jefferson, Arkansas, USA
[3]Division of the National Toxicology Program, National Institute of Environmental Health Sciences, NIH, DHHS, Research Triangle Park, North Carolina, USA
[4]National Heart, Lung, and Blood Institute, NIH, DHHS, Bethesda, Maryland, USA
[5]Social & Scientific Systems, Inc., Durham, North Carolina, USA
[6]Department of Pharmacology and Toxicology, University of Louisville School of Medicine, Louisville, Kentucky, USA
[7]National Center for Computational Toxicology, Office of Research and Development, U.S. Environmental Protection Agency, Research Triangle Park, North Carolina, USA

Background: A central challenge in toxicity testing is the large number of chemicals in commerce that lack toxicological assessment. In response, the Tox21 program is re-focusing toxicity testing from animal studies to less expensive and higher throughput *in vitro* methods using target/pathway-specific, mechanism-driven assays.

Objectives: Our objective was to use an in-depth mechanistic study approach to prioritize and characterize the chemicals affecting mitochondrial function.

Methods: We used a tiered testing approach to prioritize for more extensive testing 622 compounds identified from a primary, quantitative high-throughput screen of 8,300 unique small molecules, including drugs and industrial chemicals, as potential mitochondrial toxicants by their ability to significantly decrease the mitochondrial membrane potential (MMP). Based on results from secondary MMP assays in HepG2 cells and rat hepatocytes, 34 compounds were selected for testing in tertiary assays that included formation of reactive oxygen species (ROS), upregulation of p53 and nuclear erythroid 2-related factor 2/antioxidant response element (Nrf2/ARE), mitochondrial oxygen consumption, cellular Parkin translocation, and larval development and ATP status in the nematode *Caenorhabditis elegans*.

Results: A group of known mitochondrial complex inhibitors (e.g., rotenone) and uncouplers (e.g., chlorfenapyr), as well as potential novel complex inhibitors and uncouplers, were detected. From this study, we identified four not well-characterized potential mitochondrial toxicants (lasalocid, picoxystrobin, pinacyanol, and triclocarban) that merit additional *in vivo* characterization.

Conclusions: The tier-based approach for identifying and mechanistically characterizing mitochondrial toxicants can potentially reduce animal use in toxicological testing. https://doi.org/10.1289/EHP2589

Introduction

Humans are exposed daily to numerous naturally occurring and man-made chemicals, some of which may adversely affect health. Furthermore, each year, hundreds of new chemicals are synthesized and introduced into commercial use (https://www.epa.gov/tsca-inventory/about-tsca-chemical-substance-inventory). Currently, in the United States, more than 80,000 chemical compounds have been registered in commerce, with 15,000 used in large volume (NIEHS 2017). Toxicological profiles for most of these chemicals are inadequate or nonexistent (Dix et al. 2007). To meet the needs for rapid assessment of the potential toxicity of these chemicals, the Tox21 program, a multi-agency collaboration of the National Institutes of Health (NIH), the U.S. Environmental Protection Agency (EPA), and the Food and Drug Administration (FDA), has utilized a quantitative high-throughput screening (qHTS) approach to profile a library of ~10,000 samples (~8,300 unique structures), referred to as the Tox21 10K library, in a battery of biologically relevant cell-based assays (Kavlock et al. 2009; Shukla et al. 2010; Tice et al. 2013). Data sets generated from these assays are being used to identify mechanisms of compound action (Attene-Ramos et al. 2015; Chen et al. 2015; Hsu et al. 2014; Huang et al. 2014), prioritize chemicals for more extensive toxicological evaluation, and develop predictive models of *in vivo* biological responses (Huang et al. 2016; Judson et al. 2015; Rotroff et al. 2014).

Mitochondria play a central role in cellular metabolism including heme, fatty acid, and steroid synthesis; metabolic cell signaling; oxidative phosphorylation; Ca^{2+} homeostasis; and apoptosis (Lenaz et al. 2002; Ravagnan et al. 2002; Shaughnessy et al. 2014). Evaluating changes in mitochondrial membrane potential (MMP) using a homogenous (no wash step involved) MMP assay (Sakamuru et al. 2012) is a useful initial screen to assess for chemicals that disrupt mitochondrial function (Attene-Ramos et al. 2013, 2015). Many mitochondrial poisons are known complex inhibitors (e.g., rotenone and antimycin A) and uncouplers (e.g., 2,4-dinitrophenol and carbonyl cyamide 4-(trifluoromethoxy)phenylhydrazone, or FCCP) of oxidative phosphorylation. These chemicals cause MMP depolarization and inhibit ATP synthesis (Wallace et al. 1997). A decrease in MMP is also an early signaling event in apoptosis because depolarization of the mitochondrial membrane opens the mitochondrial permeability transition pore, which may lead to the release of

Address correspondence to M. Xia, National Institutes of Health, National Center for Advancing Translational Sciences, 9800 Medical Center Dr., Bethesda, MD 20892-3375 USA. Telephone: (301) 827-5359. Email: mxia@mail.nih.gov

Supplemental Material is available online (https://doi.org/10.1289/EHP2589).
The authors declare they have no actual or potential competing financial interests.
Received 27 July 2017; Revised 15 June 2018; Accepted 16 June 2018; Published 26 July 2018.

apoptosis initiation factors such as cytochrome c and trigger the apoptosis cascade (Marchetti et al. 1996; Zamzami et al. 1996).

Previously, we screened the Tox21 10K compound library in HepG2 cells using the MMP assay and identified 622 compounds in 76 structurally related clusters that significantly decreased MMP (Attene-Ramos et al. 2015). To prioritize this large number of compounds for further in-depth investigation, we used a tiered testing strategy (Figure 1). First, to verify the initial screening results, we retested 595 of 622 compounds for which we had sufficient remaining stock for testing in the same HepG2 MMP assay; to this group of 595 compounds, we added 27 inactive compounds structurally related to the identified active compounds (total = 622). We then screened these 622 compounds in the MMP assay using rat primary hepatocytes to identify compounds active in both cell types for further testing. Thirty-four compounds that were active in both cell types, and that represented different structurally related chemical clusters were purchased to provide independent sourcing. These 34 compounds were further investigated in the tier-two assays, which included assays that (*a*) directly measure mitochondrial function by assessing MMP in HepG2 cells, rat primary hepatocytes, and human neural stem cells (hNSC); (*b*) measure production of reactive oxygen species (ROS) as an indicator of mitochondrial damage/dysfunction; (*c*) measure pathways related to mitochondrial dysfunction by assessing up-regulation of nuclear erythroid 2-related factor 2/antioxidant response element (Nrf2/ARE) in HepG2 cells and tumor protein (p53) in HCT116 cells; (*d*) assess mitochondrial function by measuring cellular respiration in isolated rat liver mitochondria and measuring Parkin translocation as an indicator of autophagy (Sun et al. 2016) in HeLa cells; and (*e*) determine developmental effects and ATP levels in *C. elegans*. The approach we used in this tiered testing scheme provides an efficient way to prioritize compounds for more extensive toxicological evaluation while reducing the need for animal use in toxicological testing.

Materials and Methods

Cells and Culture Conditions

Human hepatocellular carcinoma cells (HepG2) were purchased from the American Type Culture Collection (ATCC). These cells were cultured in Minimum Essential (Eagle) Medium (MEM) containing 5 mM glucose (ATCC) supplemented with 10% FBS (Hyclone Laboratories) and 50 U/mL penicillin and 50 µg/mL streptomycin (Life Technologies) at 37°C in a humidified atmosphere with 5% carbon dioxide (CO_2). Plateable cryopreserved primary male rat (Sprague-Dawley) hepatocytes and CHRM® medium were obtained from Life Technologies. The rat hepatocytes were thawed in a 37°C water bath and transferred into CHRM® Medium. After centrifuging at 55 × *g* for 3 min, supernatants were removed and rat hepatocytes were resuspended in Plating Medium (Life Technologies) for use. Human neural stem cells (hNSC; H9 hESC-Derived) and culture medium were obtained from Life Technologies. To provide consistency across assays, the cell lines used in the current study were limited to those used in the HTS (high-throughput screening) assays already established in the Tox21 program.

Reagents

Mitochondrial membrane potential indicator (m-MPI), a water-soluble derivative of 5,5′,6,6′-tetrachloro-1,1′,3,3′-tetraethylbenzimidazolcarbocyanine iodide (JC-1), was obtained from

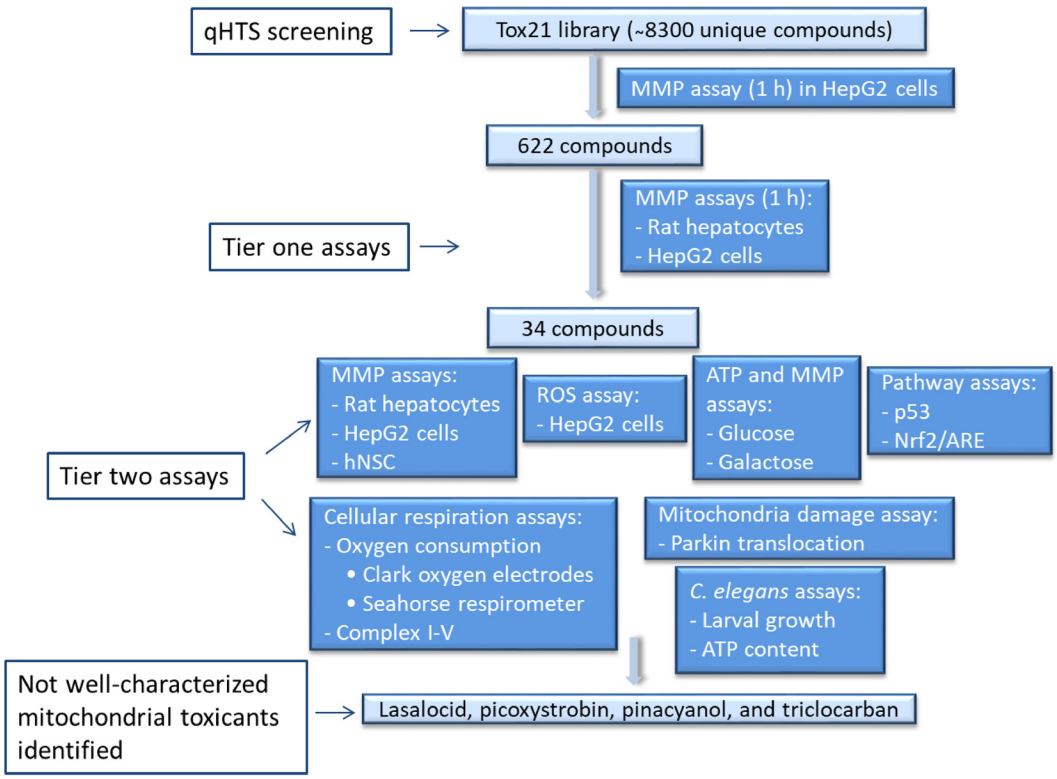

Figure 1. Compound prioritization workflow. After primary concentration–response screening (by qHTS) (Attene-Ramos et al. 2015), in which each compound was tested at 15 concentrations in three independent runs, 622 compounds were identified based on potency and efficacy in MMP assay and tested in the tier-one assays. Thirty-four compounds were selected based on the tier-one assay results and further evaluated in tier-two assays. From this prioritization via multiple assays, the 4 most potent mitochondrial toxicants (lasalocid, picoxystrobin, pinacyanol, and triclocarban), not previously tested for toxicological effects *in vivo*, were identified. Note: hNSC, human neural stem cells; MMP, mitochondrial membrane potential; Nrf2/ARE, nuclear erythroid 2-related factor 2/antioxidant response element; qHTS, quantitative high-throughput screening; ROS, reactive oxygen species.

Codex Biosolutions. A subset of 34 Tox21 compounds was purchased from Sigma-Aldrich, except for 2-hydrazino-4-(4-aminophenyl) thiazole, which was obtained from Oakwood Chemical, and lasalocid sodium purchased from Santa Cruz Biotechnology. Chemical Abstracts Service Registry Numbers (CASRN) for these 34 compounds are listed in Table 1. The purity of these compounds ranged from 95% to 98%. Tetra-octylammonium bromide (CASRN 14866–33–2; purity >98%), menadione (CASRN 58–27–5; purity ≥98%), beta-naphthoflavone (CASRN 6051–87–2; purity >98%), mitomycin C (CASRN 50–07–7; purity ≥98%), and dimethyl sulfoxide (DMSO) (CASRN 67–68–5; purity >99.7%) were obtained from Sigma-Aldrich.

Intracellular ATP Content Assay

HepG2 cells were suspended in the culture medium containing either 5 mM glucose or 10 mM galactose and seeded at 2,000 cells/5 μL per well in 1,536-well white, solid bottom plates (Greiner Bio-One) using a Multidrop Combi (Thermo Fisher Scientific). After the cells were incubated at 37°C for 5 h, 23 nL of compounds at 11 concentrations ranging from 1.6 nM to 92 μM (1.6 nM, 4.7 nM, 14 nM, 42 nM, 0.13 μM, 0.38 μM, 1.1 μM, 3.4 μM, 10 μM, 31 μM, and 92 μM final concentrations in the well) were added to the assay plates by a Wako Pintool station (Wako Automation). The assay plates were incubated for 40 h at 37°C, followed by the addition of 5 μL per well of CellTiter-Glo reagent (Promega). After a 30-min incubation at room temperature (RT), the luminescence intensity was measured using a ViewLux plate reader (PerkinElmer).

MMP Assay

The MMP assay with fluorescence readout measures changes in mitochondrial membrane potential. HepG2 cells (either in 5 mM glucose or 10 mM galactose), hNSC, or rat hepatocytes were dispensed at 2,000 cells/5 μL per well in 1,536-well black, clear-bottom assay plates (Greiner Bio-One). The plates with HepG2 and hNSC were incubated at 37°C for 18 h post seeding; rat hepatocytes were incubated for 4 h post seeding. Then, 23 nL of compounds were added to the assay plate via a Wako Pintool station. The final concentrations for the compounds are 1.6 nM, 4.7 nM, 14 nM, 42 nM, 0.13 μM, 0.38 μM, 1.1 μM, 3.4 μM, 10 μM, 31 μM, and 92 μM. The assay plates were incubated for 1 h at 37°C, followed by the addition of 5 μL/well of Dye-loading Solution (Codex Biosolutions). After the assay plates were incubated at 37°C for 30 min, fluorescence intensity (490 nm excitation and 535 nm emission for green fluorescent monomers, and 540 nm excitation and 590 nm emission for red fluorescent aggregates) was measured using an EnVision plate reader (PerkinElmer). Data were expressed as the ratio of 590:535 nm emissions.

ROS Assay

ROS-Glo™ hydrogen peroxide (H_2O_2) assay (Promega), a bioluminescent assay, measures the cellular level of H_2O_2, a ROS. HepG2 cells were seeded at 3,000 cells/5μL per well in 1,536-well white, solid-bottom plates (Greiner Bio-One) using a Multidrop Combi (Thermo Fisher Scientific). After the cells were incubated at 37°C for 18 h, 23 nL of compounds (final concentrations are 1.6 nM, 4.7 nM, 14 nM, 42 nM, 0.13 μM, 0.38 μM, 1.1 μM, 3.4 μM, 10 μM, 31 μM, and 92 μM in the assay well) were added to the assay plates using a Wako Pintool station, followed by the addition of 1 μL/well of H_2O_2 substrate solution. The positive control was menadione at 230 μM. The plates were incubated for 2 h at 37°C, followed by the addition of 4 μL/well of luciferase detection reagent. After incubation for 20 min at RT, the luminescence intensity was measured using a PerkinElmer ViewLux plate reader.

ARE and p53 β-lactamase Reporter Gene Assays

For ARE or p53 β-lactamase (*Bla*) reporter gene assays, ARE-*bla* HepG2 cells or p53-*bla* HCT-116 cells (Life Technologies) were dispensed at 2,000 cells/5 μL per well or 4,000 cells/5 μL per well, respectively, in 1,536-well black, clear-bottom plates (Greiner Bio-One). After incubation at 37°C for 6 h, 23 nL of compounds (final concentrations are 1.6 nM, 4.7 nM, 14 nM, 42 nM, 0.13 μM, 0.38 μM, 1.1 μM, 3.4 μM, 10 μM, 31 μM, and 92 μM in the assay well) were added to the assay plates using a Wako Pintool station. After 16 h incubation, 1 μL of LiveBLAzer™ (Life Technologies) detection mix was added to each well and the plates were subsequently incubated at RT for 2 h. Fluorescence intensity at 405 nm excitation and 460 and 530 nm emissions was measured by a PerkinElmer Envision plate reader. Data were represented as the ratio of the 460:530 emission values.

Oxygen Consumption Measurement

Oxygen consumption by rat liver mitochondria was measured using a pair of Clark-type oxygen electrodes integrated with the Oxytherm System from Hansatech Instruments Ltd. For mitochondrial isolation, adult male Sprague–Dawley rats (12–14 wk of age, 250–400 g body weight) from the FDA National Center for Toxicological Research (NCTR) breeding colonies were anesthetized by an intraperitoneal injection of Nembutal (Henry Schein Animal Health) and then the liver was harvested to prepare mitochondria. Animals used in the study and the procedures were approved by the FDA NCTR Institutional Animal Care and Use Committee. The combination of Nembutal anesthesia and removal of the liver as well as thoracotomy were used for euthanasia in this terminal surgical procedure. Guidelines described in the NIH's *Guide for the Care and Use of Laboratory Animals* (https://www.ncbi.nlm.nih.gov/books/NBK54050) were strictly followed throughout the study. The liver was perfused with phosphate-buffered saline (PBS) to remove blood. The liver was then cut into small pieces and homogenized using a Dounce-type homogenizer (Thermo Fisher Scientific) in ice-cold isolation buffer (IB) containing 200 mM sucrose (Sigma-Aldrich), 10 mM Tris (hydroxymethyl)aminomethane-3-(N-morpholino) propanesulfonic acid (Tris-MOPS; Sigma-Aldrich), and 1 mM ethylene-bis (oxyethylenenitrilo)tetraacetic acid (EGTA; Sigma-Aldrich) (pH 7.4). The sample was centrifuged at 600 × *g* for 10 min, the resultant supernatant was further centrifuged at 7,500 × *g* for 10 min, and the pellets were washed once with the IB and centrifuged again at 7,500 × *g* for 10 min to collect mitochondria. The concentration of freshly isolated mitochondria was adjusted to 1 mg/mL, followed by incubation with the test drug (concentrations from 1.3 nM to 100 μM) for 5 min. Then the mitochondria were divided into two equal-sized portions, to one of which was added glutamate and malate (5 and 10 mM, respectively; Sigma-Aldrich) and to the other was added succinate (5 mM; Sigma-Aldrich) to measure glutamate/malate- and succinate-driven oxygen consumption. The oxygen consumption rate with glutamate/malate or succinate was defined as state IV respiration. After 3 min, adenosine diphosphate (ADP; 200 μM; Sigma-Aldrich) was added to measure state III respiration. The ratio between state III and IV respiration rate was defined as respiratory control ratio (RCR) (Weng et al. 2015).

Oxygen consumption was also measured in HepG2 cells by the Seahorse XF24 analyzer (Seahorse Bioscience/Agilent Technologies). Briefly, measurement of intact cellular respiration was performed using the Seahorse XF24 analyzer. HepG2 cells were plated at a density of 80,000 cells/well on an XF24

Table 1. Potency (IC_{50}, μM) and efficacy (%) of active compounds re-sourced as fresh stocks and tested in the MMP assays in HepG2 cells, rat liver hepatocytes, and hNSC.

Compound	CASRN	Cluster ID	HepG2 IC_{50}, (efficacy) Glucose	Rat hepatocytes, IC_{50}, (efficacy)	hNSC, IC_{50}, (efficacy)	HepG2 IC_{50}, (efficacy) Galactose
1,4-Diaminoanthraquinone	128–95–0	21.8	0.77 ± 0.09 (−72.8 ± 4.30)	3.79 ± 1.62 (−118 ± 24.7)	0.15 ± 0.07 (−100 ± 16.5)	1.13 ± 0.14 (−78.0 ± 2.25)
1,8-Dihydroxy-4,5-dinitroanthraquinone	81–55–0	21.7	1.79 ± 0.32 (−89.3 ± 3.37)	16.09 ± 6.94 (−119 ± 28.1)	3.00 ± 0.84 (−109 ± 4.20)	2.81 ± 0.19 (−93.8 ± 3.84)
2,2′-Methylenebis(4-methyl-6-*tert*-butylphenol)	119–47–1	23.19	5.67 ± 1.02 (−93.7 ± 2.12)	6.89 ± 1.44 (−121 ± 16.7)	0.88 ± 0.25 (−114 ± 9.65)	6.60 ± 1.12 (−96.8 ± 3.14)
2,2′-Methylenebis(ethyl-6-*tert*-butylphenol)	88–24–4	23.19	5.42 ± 0.62 (−96.3 ± 6.24)	29.9 ± 7.25 (−103 ± 17.9)	1.28 ± 0.56 (−111 ± 9.68)	6.30 ± 0.43 (−96.9 ± 6.10)
2-Aminoanthraquinone	117–79–3	21.8	6.58 ± 0.90 (−73.1 ± 1.90)	9.63 ± 3.17 (−58.3 ± 7.52)	1.80 ± 0.83 (−88.7 ± 5.55)	8.98 ± 1.62 (−66.8 ± 6.16)
2-Hydrazino-4-(4-aminophenyl) thiazole	26049–71–8	22.6	15.3 ± 1.76 (−72.8 ± 3.72)	19.8 ± 11.5 (−50.5 ± 1.77)	1.76 ± 0.57 (−93.9 ± 13.0)	18.5 ± 2.55 (−66.7 ± 1.81)
2-Hydrazino-4-(4-nitrophenyl)thiazole	26049–70–7	22.6	12.1 ± 1.39 (−87.1 ± 8.73)	20.9 ± 11.3 (−73.9 ± 11.0)	4.30 ± 1.42 (−110 ± 13.1)	14.2 ± 2.56 (−90.3 ± 2.35)
2-Hydrazino-4-phenylthiazole	34176–52–8	22.6	37.1 ± 6.33 (−91.6 ± 3.54)	54.7 ± 21.1 (−57.1 ± 16.9)	14.2 ± 2.56 (−109 ± 6.54)	48.2 ± 17.5 (−96.5 ± 11.8)
5HPP-33	105624–86–0	21.2	20.1 ± 3.62 (−100 ± 2.99)	38.3 ± 4.41 (−99.8 ± 6.08)	12.1 ± 1.39 (−107 ± 4.15)	29.4 ± 5.02 (−106 ± 1.68)
Antimycin A	1397–94–0	33.6	2.79 ± 0.9 (−104 ± 3.07)	2.65 ± 1.08 (−94.9 ± 3.37)	2.91 ± 1.58 (–127 ± 14.4)	0.25 ± 0.20 (−111 ± 13.7)
Bexarotene	153559–49–0	23.19	50.0 ± 3.39 (−107 ± 4.58)	39.9 ± 5.09 (−93.8 ± 8.55)	22.3 ± 7.60 (−116 ± 5.01)	50.2 ± 6.41 (−96.2 ± 16.2)
C.I. Basic red 9 monohydrochloride	569–61–9	18.1	1.66 ± 0.28 (−97.1 ± 6.48)	6.30 ± 0.43 (−90.3 ± 2.77)	2.55 ± 0.58 (−70.3 ± 7.17)	2.53 ± 0.46 (−89.4 ± 4.30)
Chlorfenapyr	122453–73–0	25.3	1.67 ± 0.42 (−93.55 ± 4.10)	0.34 ± 0.11 (−90.8 ± 10.1)	0.13 ± 0.03 (−107 ± 15.8)	1.85 ± 0.12 (−94.9 ± 2.48)
Chlorophacinone	3691–35–8	21.17	27.1 ± 9.89 (−86.6 ± 5.34)	10.5 ± 4.28 (−97.8 ± 13.3)	12.6 ± 11.9 (−47.1 ± 19.7)	46.3 ± 3.02 (−94.7 ± 3.34)
Diclazuril	101831–37–2	29.5	38.3 ± 4.41 (−97.7 ± 7.12)	11.5 ± 5.18 (−72.8 ± 2.37)	20.6 ± 8.67 (−116 ± 15.2)	46.3 ± 3.02 (−97.6 ± 6.06)
Dinoseb	88–85–7	21.6	12.4 ± 5.84 (−98.9 ± 4.33)	4.50 ± 0.81 (−130 ± 39.0)	22.3 ± 7.60 (−148 ± 5.48)	16.5 ± 2.83 (−99.2 ± 4.31)
Dinoterb	1420–07–1	21.6	7.23 ± 2.04 (−95.6 ± 3.70)	2.39 ± 1.02 (−105 ± 23.8)	10.1 ± 2.29 (−132 ± 5.59)	7.19 ± 1.62 (−98.0 ± 3.16)
Diphenylurea	102–07–8	16.2	7.73 ± 1.62 (−108 ± 9.05)	15.4 ± 2.88 (−117 ± 8.21)	12.1 ± 1.39 (−119 ± 6.26)	10.3 ± 1.28 (−118 ± 7.86)
Emodin	518–82–1	22.19	6.14 ± 1.29 (−89.4 ± 0.55)	15.8 ± 1.07 (−106 ± 9.55)	1.09 ± 0.56 (−90.1 ± 8.03)	8.00 ± 1.44 (−88.0 ± 5.80)
FCCP	370–86–5	15.10	1.05 ± 0.38 (−95.8 ± 2.94)	0.35 ± 0.06 (−95.4 ± 4.65)	0.27 ± 0.08 (−94.2 ± 2.36)	1.12 ± 0.33 (−94.6 ± 1.13)
Lasalocid sodium	25999–20–6	35.17	1.54 ± 0.32 (−97.2 ± 3.34)	1.27 ± 0.23 (−95.6 ± 2.35)	0.54 ± 0.06 (−94.9 ± 15.3)	1.58 ± 0.11 (−95.4 ± 2.55)
Niclosamide	50–65–7	20.1	0.87 ± 0.33 (−91.6 ± 2.07)	1.36 ± 0.16 (−107 ± 13.5)	0.42 ± 0.20 (−110 ± 9.75)	1.47 ± 0.20 (−96.4 ± 3.55)
Niflumic acid	4394–00–7	28.3	44.6 ± 3.02 (−82.0 ± 8 .64)	19.9 ± 1.35 (−98.8 ± 9.27)	38.3 ± 4.41 (−118 ± 10.5)	42.8 ± 0.00 (−69.4 ± 9.92)
Palmatine chloride hydrate	171869–95–7	32.9	55.7 ± 17.9 (−42.0 ± 2.98)	6.74 ± 2.89 (−101 ± 2.09)	34.1 ± 11.2 (−75.8 ± 21.0)	70.6 ± 4.79 (−47.6 ± 2.55)
Picoxystrobin	117428–22–5	30.8	13.6 ± 14.5 (−62.9 ± 25.1)	16.1 ± 7.03 (−77.3 ± 9.18)	38.2 ± 0.00 (−92.8 ± 16.3)	24.4 ± 4.56 (−119 ± 6.45)
Pinacyanol chloride	605–91–4	20.9	0.04 ± 0.01 (−85.9 ± 3.17)	0.31 ± 0.15 (−75.4 ± 6.24)	0.04 ± 0.01 (−97.1 ± 7.31)	0.06 ± 0.02 (−78.9 ± 0.48)
Rafoxanide	22662–39–1	32.7	20.9 ± 11.3 (−97.4 ± 5.32)	4.50 ± 0.81 (−72.1 ± 10.3)	10.3 ± 3.40 (−100 ± 4.78)	18.6 ± 3.17 (−97.3 ± 4.00)
Rhein	478–43–3	22.19	15.2 ± 1.76 (−26.3 ± 5.13)	6.76 ± 4.03 (−37.5 ± 6.05)	10.3 ± 3.40 (−54.8 ± 6.68)	Inactive
Rifampicin	13292–46–1	33.6	63.2 ± 8.07 (−66.2 ± 20.9)	41.4 ± 5.71 (−97.5 ± 6.10)	37.1 ± 6.33 (−95.5 ± 7.91)	Inactive
Rifapentine	61379–65–5	33.6	13.9 ± 3.89 (−95.7 ± 3.54)	5.94 ± 1.48 (−73.4 ± 10.2)	8.07 ± 1.82 (−92.1 ± 5.79)	17.7 ± 1.20 (−90.3 ± 5.02)
Rotenone	83–79–4	34.14	44.7 ± 5.71 (−89.4 ± 17.4)	0.36 ± 0.22 (−85.9 ± 10.7)	23.7 ± 38.2 (−81.1 ± 14.2)	31.8 ± 5.73 (−106 ± 11.2)
Thidiazuron	51707–55–2	16.2	12.0 ± 0.00 (−101 ± 2.07)	14.7 ± 2.52 (−98.5 ± 15.2)	8.39 ± 2.10 (−114 ± 20.4)	14.6 ± 0.95 (−105 ± 4.56)
Triclocarban	101–20–2	9.5	0.93 ± 0.37 (−104 ± 0.63)	1.77 ± 0.60 (−73.7 ± 3.11)	0.43 ± 0.08 (−91.3 ± 11.6)	1.36 ± 0.16 (−104 ± 2.60)
Triethyltin bromide	2767–54–6	2.12	0.65 ± 0.21 (−103 ± 3.17)	2.54 ± 0.95 (−90.5 ± 2.33)	1.28 ± 0.55 (−91.5 ± 14.5)	1.46 ± 0.61 (−97.4 ± 2.53)

Note: Each value of potency (IC_{50}, μM) and efficacy [percentage (%) of positive control, expressed in parentheses] is the mean ± SD of the results from three experiments. CASRN, Chemical Abstracts Service Registry Number; Cluster ID, coordinates of the cluster on the SOM map (Attene-Ramos et al. 2015), where the first number is the row number and the second number is the column number on the map; hNSC, human Neural Stem Cells; FCCP, carbonyl cyamide 4-(trifluoromethoxy)phenylhydrazone; IC_{50}, concentration of half-maximal inhibition; MMP, mitochondrial membrane potential.

tissue culture plate (Seahorse Bioscience/Agilent Technologies), and cultured overnight in Dulbecco's Modified Eagle's Medium (DMEM; Corning Life Sciences) supplemented with 10% FBS, 50 U/mL penicillin and 50 μg/mL streptomycin (Life Technologies). Prior to the respiration assay, cells were rinsed and cultured in DMEM running medium (Sigma-Aldrich), 200 mM GlutaMax-1 (Life Technologies), 100 mM sodium pyruvate, 25 mM D-glucose, 63.3 mM sodium chloride (NaCl), and phenol red (Sigma-Aldrich), with the pH adjusted to 7.4 according to the manufacturer's protocol. Respiration was measured under the basal condition and in the presence of four different concentrations (1, 4, 16, and 64 μM) of the compounds in order to assess oxidative capacity. Respiration was routinely measured using 25 mM glucose as the extracellular substrate.

Measurement of Respiratory Chain Complex Activities

Respiratory chain complex (RCC) I–V activities were determined using previously published procedures (Kirby et al. 2007; Weng et al. 2014). Submitochondrial particles were prepared by subjecting the intact rat mitochondria, isolated as described above, to three successive freeze–thaw cycles (Kirby et al. 2007). Test compounds were incubated with submitochondrial particles (1 mg/mL) for 15 min and then RCC I–V activities were measured. The activities of DMSO-treated samples (controls) were set as 1. RCC I activity was measured using a buffer containing 25 mM potassium phosphate (KH_2PO_4/K_2HPO_4); 5 mM magnesium chloride ($MgCl_2$), pH 7.2, 0.25% bovine serum albumin (BSA; Sigma-Aldrich); 0.13 mM β-nicotinamide adenine dinucleotide, reduced dipotassium salt (NADH, Sigma-Aldrich); 2 mM potassium cyanide (KCN, Sigma-Aldrich); 2 μg/mL antimycin A (Sigma-Aldrich); and 65 μM ubiquinone 1 (Sigma-Aldrich), which was supplemented with or without 2 μg/mL rotenone (Sigma-Aldrich). The difference between the activity using the rotenone-containing buffer and rotenone-absent buffer was considered as RCC I activity. RCC II activity was measured in a buffer containing 25 mM KH_2PO_4/K_2HPO_4; 5 mM $MgCl_2$, pH 7.2, 20 mM sodium succinate (Sigma-Aldrich); 50 μM 2,6-dichloroindophenol sodium salt hydrate (Sigma-Aldrich); 2 mM KCN; 2 μg/mL antimycin A; 2 μg/mL rotenone; and 65 μM ubiquinone 1. RCC III activity was determined with a buffer containing 25 mM KH_2PO_4/K_2HPO_4, pH 7.2, 1 mM *n*-dodecyl-β-D-maltoside (Sigma-Aldrich); 1 mM KCN; 1 μg/mL rotenone; 100 μM reduced-decylubiquinone; 15 μM oxidized cytochrome c (Sigma-Aldrich); and 0.1% BSA. RCC IV activity was measured using a buffer containing 25 mM KH_2PO_4/K_2HPO_4, pH 7.2; 1 mM *n*-dodecyl-β-D-maltoside; and 15 μM reduced cytochrome c. RCC V was measured with a buffer containing 40 mM Tris; 10 mM ethylene glycol-bis(β-aminoethyl ether)-*N,N,N′,N′*-tetraacetic acid (EGTA), pH 8.0; 0.2 mM NADH; 2.5 mM phospho(enol)pyruvic acid monopotassium salt (Sigma-Aldrich); 2.5 μg/mL antimycin A; 5 mM $MgCl_2$; 5 U/mL lactate dehydrogenase (Sigma-Aldrich); 5 U/mL pyruvate kinase (Sigma-Aldrich); and 2.5 mM ATP (Sigma-Aldrich), which was supplemented with or without 2 μg/mL oligomycin A. The difference between the activity using the oligomycin A–containing buffer and the oligomycin A–absent buffer was considered as RCC V activity. For measuring RCC I/V and II activity, the changes in absorbance at 340 nm and 600 nm, respectively, were determined every 1 min for 6 min. For measuring RCC III and RCC IV, the changes in absorbance at 550 nm were measured every 10 s for 2 min. A Synergy 2 Multi-Mode microplate reader from BioTek was used for these measurements.

Parkin Translocation

Confocal experiments were performed using a recently described HeLa cell line stably expressing YFP-Parkin (Nezich et al. 2015) plated on 35 mm coverglass #1.5 chamber dishes (MatTek), in DMEM containing 10% FBS supplemented with 100 U/mL penicillin and 100 μg/mL streptomycin (Life Technologies). These cells were treated for 2 h with DMSO as vehicle control or with tested compounds at indicated concentrations. Fluorescent samples of YFP-Parkin were routinely examined with a Zeiss LSM 780 confocal microscope (Carl Zeiss) as previously described (Sun et al. 2015). YFP was imaged with a 514-nm excitation and 520- to 570-emission filters.

Data Analysis for MMP, ROS, Viability, ARE, and p53 Assays

Analysis of compound concentration–response data was performed as previously described (Huang 2016). Briefly, raw plate reads for each titration point were first normalized relative to the positive control compound (−100% for antagonist mode and 100% for agonist mode) and DMSO-only wells (0%) as follows: $\%\,\text{Activity} = [(\text{Vcompound} - V_{DMSO})/(\text{Vpos} - V_{DMSO})] \times 100$ (in which Vcompound denotes the compound well values, Vpos denotes the median value of the positive control wells, and V_{DMSO} denotes the median values of the DMSO-only wells) and then corrected by applying an NCATS in-house pattern correction algorithm (Wang and Huang 2016) using compound-free control plates (i.e., DMSO-only plates) at the beginning and end of the compound plate stack. Concentration–response titration points for each compound were fitted to a four-parameter Hill equation yielding concentrations of half-maximal inhibitory activity (IC_{50}) or half-maximal stimulatory activity (EC_{50}) and maximal response (efficacy) values (Wang et al. 2010). Compounds were designated as Class 1–4 according to the type of concentration–response curve observed (Huang 2016). Each compound was assigned an activity outcome based on its type of concentration–response curve and reproducibility as described previously (Attene-Ramos et al. 2015). Compounds that showed a reproducible concentration response were classified as active (Huang 2016). Compounds from the Tox21 library were clustered based on structural similarity (512-bit ChemAxon® Chemical Fingerprints (version 6.2.1; ChemAxon) using the self-organizing map (SOM) algorithm (Kohonen 2006), yielding 651 clusters. Each cluster was evaluated for its enrichment of active antagonists (compared with the library average) using Fisher's Exact Test. For confirmation and follow-up studies to the HepG2 cell MMP results, compounds were selected from 302 clusters that contained at least one active antagonist based on activity outcome (active antagonist), potency (<10 μM; <50 μM close structure analogs), efficacy (>50%), and research interest (e.g., drugs with known toxicity). In addition to active compounds, one or two inactive close structural analogs were also selected from clusters that were enriched with active antagonists in order to test for potential false negative outcomes. The Pearson correlations of the IC_{50} values among hNSC, HepG2 cells, and rat primary hepatocytes were measured using GraphPad Prism 7 (GraphPad Software, Inc.).

Nematode Culture

Bristol N2 (wild type) *Caenorhabditis elegans* obtained from the *Caenorhabditis* Genetic Center were used in the larval development and growth assay. The transgenic *C. elegans* strain PE255 [*sur-5::luc+::gfp; rol-6(su1006)*] used in the ATP assay (Lagido et al. 2009) was also obtained from the *Caenorhabditis* Genetic Center; this strain expresses luciferase to measure *in vivo* ATP levels and GFP (green fluorescent protein) as a marker of live animals. All nematodes were maintained at 20°C on K-agar plates seeded with OP50 *Escherichia coli* (*Caenorhabditis* Genetic Center) as a food

source (Williams and Dusenbery 1988), or as age-synchronized cultures of first stage larvae (L1s) by hatching embryos in the absence of food, causing L1 development to arrest, as previously described (Boyd et al. 2009). The K-agar plates are made at NIEHS from 2% bacto-agar, 0.25% bacto-peptone, 51 mM sodium chloride, 32 mM potassium chloride, and 13 μM cholesterol (Sigma-Aldrich); complete K-medium consists of 51 mM sodium chloride, 32 mM potassium chloride, 3 mM calcium chloride, 3 mM magnesium sulfate, and 13 μM cholesterol was also made at NIEHS.

Chemical exposures for C. elegans *Experiments*

The chemical compounds were initially tested at identical concentrations (0.5, 1, 2.5, 5, 10, 25, 50, 75, and 100 μM) in *C. elegans* experiments. Several compounds were tested at additional lower concentrations until no effect on development was observed (i.e., a no-observable-effect-concentration, or NOEC, was reached). The additional compounds tested at lower concentrations were chlorfenapyr, rotenone, triclocarban, and triethyltin bromide at 0.25, 0.1, and 0.05 μM; and pinacyanol chloride, tested at 0.25, 0.1, 0.05, 0.05, 0.025, 0.01, and 0.005 μM. All compound exposures including vehicle and positive controls were replicated across 6 wells on each 96-well treatment plate.

Larval Development and Growth

C. elegans larval development and growth assays were performed as previously described (Union Biometrica Inc.) (Boyd et al. 2016). Briefly, 50 L1 nematodes were dispensed to each exposure well of a 96-well plate containing the test compound, DMSO (1% final concentration), *E. coli*, and complete K-medium. Nematodes were exposed to compounds at 20°C for 48 h, conditions in which untreated nematodes developed to the final larval stage (L4s). After the incubation, the gross morphology and developmental stage of the nematodes were visually assessed by microscopy. The number of animals and size of individual nematodes were then determined using the Biosort. Nematode size is expressed as extinction (EXT), which is a measure of the optical density over the length of each animal. Measurements of extraneous material such as detritus, bacteria clumps, or precipitates were mathematically filtered from the data using a growth model, as previously described (Boyd et al. 2010; Smith et al. 2009). The average log(EXT) value for each well was used for subsequent analyses.

In vivo C. elegans ATP Status

For the ATP assay, age-synchronized L1s were transferred to culture plates with food and allowed to develop for 24 h to the late L2/early L3 stage. Larvae were rinsed from culture plates and 50 larvae were dispensed using a Biosort to each well of white 96-well plates (Greiner Lumitrac). Nematodes were exposed to compounds for 24 h with untreated animals reaching the L4 stage, as described for the development assay. After exposure, green fluorescence and luminescence were measured using a FLUostar Optima plate reader (BMG Labtech Inc.). Fluorescence was read at 485 nm excitation and 520 nm emission. To measure ATP, luminescence buffer [0.1 mM D-luciferin (Life Technologies), 1% DMSO, 5% Triton-X (Fluka BioChemika), 0.1 mM citric acid (Sigma-Aldrich), and 0.2 mM dibasic sodium phosphate (Sigma-Aldrich)] was injected into each well. After 3 min, luminescence was read at 570 nm using the Optima plate reader.

Data analyses for C. elegans Experiments

The two assays were analyzed similarly. In each case, plate adjustments were made by subtracting the well means of the test compounds from the overall mean of the plate controls. Lowest effect concentrations (LECs) were found using *t*-tests to compare observations of test compounds against plate vehicle controls (1% DMSO). Bonferroni corrections were made to ensure an overall significance level of 0.05 of the LEC calculations for each assay.

Results

Identification of Compounds That Decreased MMP

Approximately 8,300 unique chemicals in 651 structure-related clusters comprising the Tox21 10K library were previously screened for effects on MMP using a cell-based MMP assay (Attene-Ramos et al. 2015). From this primary qHTS screening, in which compounds were tested at 15 concentrations at three independent times (Attene-Ramos et al. 2015), we selected 622 compounds (595 compounds classified as active and 27 compounds classified as inactive yet structurally related to active compounds) representing 72 structure clusters based on compound potency, efficacy, and chemical structure (see "Data analysis for MMP assay" in the "Methods" section for details). Among the compounds that decreased MMP were several well-known mitochondrial toxicants including FCCP and antimycin A. We retested the 622 compounds in the HepG2 cell MMP assay using existing Tox21 10K library stock solutions. Of the 595 compounds that were previously identified as active, 543 (91%) were active in the current analysis. Of the 27 compounds that were previously identified as inactive, 24 (89%) were inactive in the current analysis (see Excel Table S1). To characterize the activity of the compounds in different species in order to prioritize compounds for more extensive characterization, these compounds were also evaluated in a rat primary hepatocyte-MMP assay (1-h treatment). Among the 567 compounds with confirmed activity (active or inactive) in the HepG2 cell MMP assay, 426 were also active (406/543, 75%) or inactive (20/24, 83%) in the rat hepatocyte-MMP assay (see Excel Table S1). As shown in Excel Table S1, pinacyanol chloride was the most potent active compound, based on having the lowest IC_{50} values in one of the two assays, with IC_{50} of 0.04 and 0.02 μM in rat primary hepatocytes and HepG2 cells, respectively, followed by chlorfenapyr (0.07 μM in rat hepatocytes, 0.04 μM in HepG2 cells), gramicidin (0.2 μM in rat hepatocytes, 0.04 μM in HepG2 cells), triclocarban (0.17 μM in rat hepatocytes, 0.17 μM in HepG2 cells), 2,6-di-*tert*-butyl-4-nitrophenol (0.29 μM in rat hepatocytes, 0.11 μM in HepG2 cells), niclosamide (0.44 μM in rat hepatocytes, 0.10 μM in HepG2 cells), and fluorosalan (0.42 μM in rat hepatocytes, 0.19 μM in HepG2 cells). Based on cutoffs for potency ($IC_{50} \leq 10$ μM) and efficacy (>50% of positive control) in both rat primary hepatocyte and HepG2 cell MMP assays, 90 compounds were found to meet these criteria. Then based on novelty, structural cluster, and commercial availability, 34 compounds—representing 24 chemical structure clusters—were selected and repurchased from commercial vendors for further characterization (Table 1).

Confirmatory and Mechanistic Studies of Compounds That Decreased MMP

To further characterize their ability to decrease MMP, the 34 selected compounds, including the positive controls FCCP and antimycin A, were re-tested in the MMP assays using HepG2 cells and rat primary hepatocytes, and tested also in hNSC. As shown in Table 1, all of the compounds tested inhibited MMP in all three cell types tested, and some of these compounds, such as antimycin A, lasalocid, rifampicin, rifapentine, and thidiazuron, exhibited similar potencies across the three cell types. The IC_{50} values of these compounds were highly correlated between

hNSC and HepG2 cells (Pearson correlation: $R = 0.89$), whereas the correlation between the IC_{50} values in rat primary hepatocytes with either hNSC or HepG2 cells was lower ($R = 0.59$ with hNSC, $R = 0.62$ with HepG2 cells) as shown in Figure S1. Of note, rotenone had a higher potency ($IC_{50} = 0.36$ μM) in rat primary hepatocytes than did hNSC ($IC_{50} = 23.7$ μM) and HepG2 cells ($IC_{50} = 44.7$ μM), whereas pinacyanol was more potent in hNSC ($IC_{50} = 0.04$ μM) and HepG2 cell ($IC_{50} = 0.04$ μM) than rat primary hepatocytes ($IC_{50} = 0.31$ μM). In general, the two human cell lines exhibited similar sensitivity but were generally more sensitive than rat primary hepatocytes to the effects of these 34 chemicals on MMP.

To further characterize their ability to decrease MMP, these 34 compounds were tested for their ability to decrease intracellular ATP content. Of these 34 compounds tested in the cell viability assay measuring intracellular ATP content using 5 mM glucose as the energy source, 27 induced a decrease in ATP content (Table 2). We further evaluated the ability of these compounds to decrease MMP (Table 1) and viability/ATP content (Table 2) in HepG2 cells cultured in galactose (no glucose, 10 mM galactose), a growth condition that enhances dependence on oxidative phosphorylation pathways and, hence, sensitivity to mitochondrial toxicants. Most of the compounds had similar activity under both galactose (10 mM) and low glucose (5 mM) conditions ($R = 0.95$ in MMP assay and $R = 0.96$ in the viability/ATP assay); the only exception was antimycin A, which was more potent in the MMP assay with galactose treatment compared with low glucose treatment.

We then characterized the ability of the compounds to induce ROS in HepG2 cells. As shown in Table 2, 22 of 34 compounds induced ROS production in HepG2 cells, with EC_{50} values ranging from 1.93 to 41.7 μM. Of these, 8 compounds had EC_{50} values <10 μM, with rank order of potency (EC_{50} values) of chlorfenapyr (1.93 μM), FCCP (2.49 μM), rotenone (4.04 μM), 2-aminoanthraquinone (4.72 μM), emodin (5.24 μM), niflumic acid (6.35 μM), triethyltin bromide (6.46 μM), and antimycin A (6.83 μM).

Several cellular stress pathways including p53 and Nrf2/ARE have been linked to mitochondrial dysfunction (Dinkova-Kostova and Abramov 2015; Mammucari and Rizzuto 2010). To investigate effects on p53 and Nrf2/ARE signaling pathways, the 34 compounds identified as active in the MMP assay were tested in the p53-*bla* and Nrf2/ARE-*bla* assays. Many of these compounds—such as antimycin A, diclazuril, dinoseb, emodin, triclocarban, and triethyltin bromide—induced both signaling pathways with similar potencies, although some of the compounds—including 5HPP-33, dinoterb, picoxystrobin, and rotenone—had different EC_{50} values in these two assays (Table 2). Other compounds activated only the p53 pathway—including niclosamide, rafoxanide, and chlorfenapyr—or the Nrf2/ARE pathway—including pinacyanol, 1,8-dihydroxy-4,5-dinitroanthraquinone, 2-aminoanthraquinone, 2-hydrazino-4-(4-aminophenyl) thiazole, 2-hydrazino-4-(4-nitrophenyl)thiazole, and 2-hydrazino-4-phenylthiazole (Table 2).

Effect of Compounds on Mitochondrial Respiration

Oxygen consumption and complex I–V activity are directly related to mitochondrial function, specifically mitochondrial toxicity. Mitochondrial oxygen consumption was measured using the traditional Clark-type oxygen electrode after treatment of isolated rat liver mitochondria with each of the 34 compounds at concentrations up to 100 μM. FCCP, a known mitochondrial electron transport uncoupler, significantly increased the glutamate/malate-driven state 4 respiration in a concentration-dependent manner, with a maximal increase of approximately 4-fold over the baseline level at 0.8 μM, but only slightly affected the glutamate/malate-driven state 3 respiration (Figure 2A). The corresponding RCR after FCCP treatment began to decrease at 32 nM and reached unity, indicating a complete uncoupling, at 4 μM (Figure 2A). FCCP also increased succinate-driven state 4 respiration in a concentration-dependent manner (Figure 2B), with a maximal 2.6-fold response over the baseline level at 0.16 μM, but did not affect state 3 respiration at this concentration. Of the 34 compounds tested, 23 compounds (see Excel Table S2), such as chlorfenapyr (Figure 2C,D), dinoterb (Figure 2E,F), and triclocarban (Figure 2G,H), had effects similar to those of FCCP. Five compounds had an inhibitory effect on respiration. For example, antimycin A, a known complex III inhibitor, significantly inhibited both glutamate/malate-driven respiration and succinate-driven respiration (Figure 3A,B). In contrast, rotenone, a known complex I inhibitor, only inhibited glutamate/malate-driven respiration, but not succinate-driven respiration (Figure 3C,D). Picoxystrobin (Figure 3E,F) had effects similar to antimycin A, although pinacyanol chloride (Figure 3G,H) had slightly milder inhibitory effects on both glutamate/malate-driven respiration and succinate-driven respiration. C.I. Basic Red 9 monohydrochloride (Figure 3I,J), only had moderate inhibitory effect on state 3 respiration driven by both glutamate/malate and succinate, but not on state 4 respiration. The remaining 6 compounds were inactive in the oxygen consumption assay (see Excel Table S2). The 34 compounds were also analyzed for their effects on oxygen consumption rate using a Seahorse XF24 respirometer (Table 3; see also Figure S2). Again, for example, chlorfenapyr demonstrated effects similar to that of FCCP (Figure 4A), whereas pinacyanol chloride produced inhibitory patterns similar to that of rotenone (Figure 4B). The concentrations that elicited an effect in the Seahorse experiments (Figure 4A) correlated well with the concentrations that showed activity in isolated mitochondria (Figure 2).

To further study the effect of these inhibitors on the respiratory complex, 11 compounds, identified either as inhibitors or uncouplers/inhibitors using the Clark-type oxygen electrode method (see Excel Table S2), were tested on complex I, II, III, IV, and V activity. As shown in Table 4, 10 of these 11 compounds inhibited one or more complexes. For example, rotenone and pinacyanol specifically inhibited complex I in a concentration-dependent manner (Figure 5A). Rafoxanide inhibited both complex II (Figure 5B) and complex V (Figure 5C), whereas picoxystrobin inhibited both complex I (Figure 5A) and complex III (Figure 5D). Antimycin A inhibited only complex III (Figure 5D), but triethyltin bromide inhibited complex V (Figure 5C). None of these compounds inhibited complex IV (Table 4).

Effect of Compounds on Mitochondrial Damage and Parkin Translocation

To further characterize the mitochondrial toxicity of the 34 chemicals, their ability to enhance cellular Parkin translocation was tested in HeLa cells expressing YFP-Parkin. Of these 34 chemicals, 12 induced Parkin translocation (Table 3). Compared with the DMSO solvent control (Figure 6A), the positive controls, FCCP (Figure 6B) and antimycin A (Figure 6C), also significantly increased Parkin translocation into mitochondria. Similarly, chlorfenapyr (Figure 6D), dinoterb (Figure 6E), and pinacyanol (Figure 6F) showed patterns similar to antimycin A and FCCP. In contrast, rotenone (Figure 6G) and picoxystronbin (Figure 6H) did not induce Parkin translocation.

In vivo studies in *C. elegans*

To determine whether the effects of these mitochondrial toxicants observed in cell culture could be recapitulated under *in vivo* conditions, *C. elegans* was used as an *in vivo* model to test the ability of the 34 compounds over a concentration range of 0.5–100 μM

Table 2. Compound potency (EC_{50} or IC_{50}, μM) and efficacy (%) from ROS, intracellular ATP content, p53, and ARE assays.

Compound	ROS (HepG2), EC_{50}, (efficacy)	ATP (HepG2, glucose), IC_{50}, (efficacy)	ATP (HepG2, galactose), IC_{50}, (efficacy)	p53 (HCT-116), EC_{50}, (efficacy)	ARE (HepG2), EC_{50}, (efficacy)
1,4-Diaminoanthraquinone	Inactive	24.7 ± 9.69 (−70.9 ± 13.4)	22.3 ± 1.51 (−68.5 ± 11.5)	35.7 ± 2.41 (51.8 ± 10.5)	22.9 ± 27.4 (46.9 ± 25.0)
1,8-Dihydroxy-4,5-dinitroanthraquinone	34.3 ± 0.00 (78.1 ± 12.6)	27.0 ± 13.6 (−116 ± 4.31)	17.0 ± 0.00 (−115 ± 3.27)	Inactive	2.43 ± 1.38 (87.7 ± 9.21)
2,2′-Methylenebis(4-methyl-6-*tert*-butylphenol)	31.4 ± 10.1 (27.5 ± 4.98)	34.1 ± 3.93 (−107 ± 8.64)	34.0 ± 0.00 (−115 ± 5.47)	Inactive	Inactive
2,2′-Methylenebis(ethyl-6-*tert*-butylphenol)	29.6 ± 4.08 (18.2 ± 6.62)	21.6 ± 13.79 (−79.9 ± 48.3)	29.8 ± 7.25 (−95.9 ± 10.0)	Inactive	Inactive
2-Aminoanthraquinone	4.72 ± 0.80 (41.7 ± 13.3)	Inactive	Inactive	Inactive	3.93 ± 0.89 (33.9 ± 12.8)
2-Hydrazino-4-(4-aminophenyl) thiazole	25.4 ± 3.24 (41.4 ± 3.65)	59.5 ± 23.5 (−61.9 ± 19.5)	60.8 ± 6.99 (−51.5 ± 10.9)	Inactive	10.5 ± 8.10 (39.2 ± 7.15)
2-Hydrazino-4-(4-nitrophenyl)thiazole	15.4 ± 16.6 (19.7 ± 9.67)	48.1 ± 24.3 (−48.0 ± 27.3)	35.5 ± 4.54 (−49.8 ± 9.75)	Inactive	9.83 ± 3.79 (42.9 ± 15.7)
2-Hydrazino-4-phenylthiazole	34.5 ± 28.8 (19.9 ± 9.56)	Inactive	Inactive	Inactive	6.92 ± 1.73 (34.2 ± 3.19)
5HPP-33	37.1 ± 2.42 (37.6 ± 1.63)	51.2 ± 14.4 (−67.7 ± 3.67)	39.7 ± 2.69 (−66.5 ± 7.10)	1.73 ± 0.19 (76.9 ± 9.78)	25.3 ± 1.74 (54.9 ± 7.97)
Antimycin A	6.83 ± 4.53 (43.9 ± 4.55)	0.02 ± 0.02 (−89.3 ± 4.02)	0.05 ± 0.05 (−88.2 ± 5.50)	0.31 ± 0.04 (36.8 ± 6.84)	0.47 ± 0.42 (33.7 ± 12.0)
Bexarotene	Inactive	63.2 ± 8.07 (−100 ± 31.5)	63.2 ± 8.07 (−81.2 ± 49.3)	Inactive	11.5 ± 0.75 (67.2 ± 19.4)
C.I. Basic red 9 monohydrochloride	Inactive	9.72 ± 5.01 (−101 ± 8.17)	6.25 ± 2.01 (−98.4 ± 12.9)	Inactive	11.7 ± 7.37 (107 ± 42.3)
Chlorfenapyr	1.93 ± 0.98 (40.7 ± 5.38)	6.41 ± 1.45 (−90.0 ± 9.60)	7.01 ± 2.94 (−86.9 ± 15.8)	10.5 ± 3.43 (31.4 ± 1.92)	Inactive
Chlorophacinone	41.7 ± 2.71 (146 ± 10.0)	48.2 ± 17.5 (−78.4 ± 12.2)	41.4 ± 5.71 (−71.8 ± 10.3)	Inactive	Inactive
Diclazuril	Inactive	50.4 ± 9.08 (−32.0 ± 7.76)	43.4 ± 9.10 (−33.7 ± 10.9)	27.9 ± 6.48 (31.6 ± 8.08)	10.9 ± 0.00 (50 ± 9.76)
Dinoseb	27.6 ± 5.16 (32.9 ± 4.14)	36.8 ± 2.40 (−90.1 ± 15.2)	32.6 ± 9.65 (−95.4 ± 17.3)	2.63 ± 1.78 (27.6 ± 13.6)	0.76 ± 0.13 (48.3 ± 10.3)
Dinoterb	13.2 ± 0.86 (35.1 ± 3.18)	19.7 ± 5.49 (− 94.5 ± 22.3)	22.3 ± 11.1 (−100 ± 30.6)	15.5 ± 7.14 (57.3 ± 9.23)	0.52 ± 0.15 (57.7 ± 16.7)
Diphenylurea	Inactive	Inactive	Inactive	Inactive	Inactive
Emodin	5.24 ± 1.72 (57.8 ± 11.9)	43.0 ± 4.95 (−82.0 ± 6.57)	39.7 ± 2.69 (−76.0 ± 17.4)	14.9 ± 6.50 (34.3 ± 17.9)	10.5 ± 1.45 (103 ± 32.4)
FCCP	2.49 ± 0.45 (35.9 ± 5.66)	2.90 ± 0.72 (−90.1 ± 9.46)	4.25 ± 0.97 (−91.9 ± 3.75)	Inactive	Inactive
Lasalocid sodium	Inactive	30.7 ± 5.74 (−116 ± 10.9)	35.4 ± 12.0 (−116 ± 9.36)	Inactive	Inactive
Niclosamide	Inactive	2.01 ± 0.36 (−91.0 ± 15.4)	2.26 ± 0.41 (−92.5 ± 14.6)	0.58 ± 0.49 (28.7 ± 11.1)	Inactive
Niflumic acid	6.35 ± 2.16 (61.7 ± 13.8)	Inactive	Inactive	Inactive	25.1 ± 2.05 (41.5 ± 2.54)
Palmatine chloride hydrate	Inactive	19.0 ± 9.49 (−24.2 ± 13.1)	27.1 ± 8.93 (−37.1 ± 13.9)	Inactive	Inactive
Picoxystrobin	15.4 ± 5.47 (36.2 ± 2.46)	3.61 ± 1.57 (−76.4 ± 30.3)	3.08 ± 0.64 (−76.4 ± 37.7)	6.68 ± 2.21 (40.2 ± 19.6)	0.75 ± 0.49 (57.6 ± 7.85)
Pinacyanol	Inactive	10.7 ± 6.39 (−107 ± 6.73)	5.88 ± 2.33 (−105 ± 4.87)	Inactive	1.39 ± 0.95 (62.8 ± 13.4)
Rafoxanide	26.5 ± 4.52 (44.2 ± 4.63)	46.7 ± 7.96 (−98.3 ± 9.95)	54.1 ± 17.8 (−107 ± 21.3)	9.11 ± 3.81 (44.3 ± 6.58)	Inactive
Rhein	Inactive	Inactive	Inactive	Inactive	15.4 ± 8.38 (85.6 ± 17.3)
Rifampicin	34.5 ± 3.96 (110 ± 53.1)	Inactive	Inactive	Inactive	45.2 ± 5.76 (42.0 ± 5.74)
Rifapentine	Inactive	43.4 ± 9.10 (−59.6 ± 28.9)	36.0 ± 8.13 (−59.8 ± 12.1)	Inactive	29.3 ± 7.09 (70.8 ± 36.6)
Rotenone	4.04 ± 1.98 (60.6 ± 10.5)	1.05 ± 1.72 (−98.9 ± 24.0)	1.63 ± 2.75 (−98.7 ± 9.31)	0.43 ± 0.11 (50.1 ± 13.1)	0.05 ± 0.02 (47.7 ± 3.64)
Thidiazuron	Inactive	Inactive	Inactive	Inactive	27.3 ± 9.74 (37.6 ± 8.81)
Triclocarban	31.8 ± 2.16 (32.9 ± 6.11)	19.1 ± 6.83 (−84.1 ± 12.4)	15.8 ± 1.07 (−91.2 ± 11.2)	5.33 ± 2.02 (33.5 ± 12.7)	6.68 ± 0 (82.6 ± 6.83)
Triethyltin bromide	6.46 ± 1.46 (48.6 ± 11.0)	6.61 ± 9.07 (−100 ± 9.47)	1.45 ± 0.43 (−94.5 ± 3.90)	2.16 ± 0.00 (64.4 ± 4.95)	2.64 ± 0.36 (91.3 ± 24.9)

Note: Each value of potency (EC_{50} or IC_{50}, μM) and efficacy (% of positive control, expressed in parentheses) is the mean ± SD of the results from three experiments. EC_{50}, concentration of half-maximal activation; FCCP, carbonyl cyamide 4-(trifluoromethoxy)phenylhydrazone; IC_{50}, concentration of half-maximal inhibition.

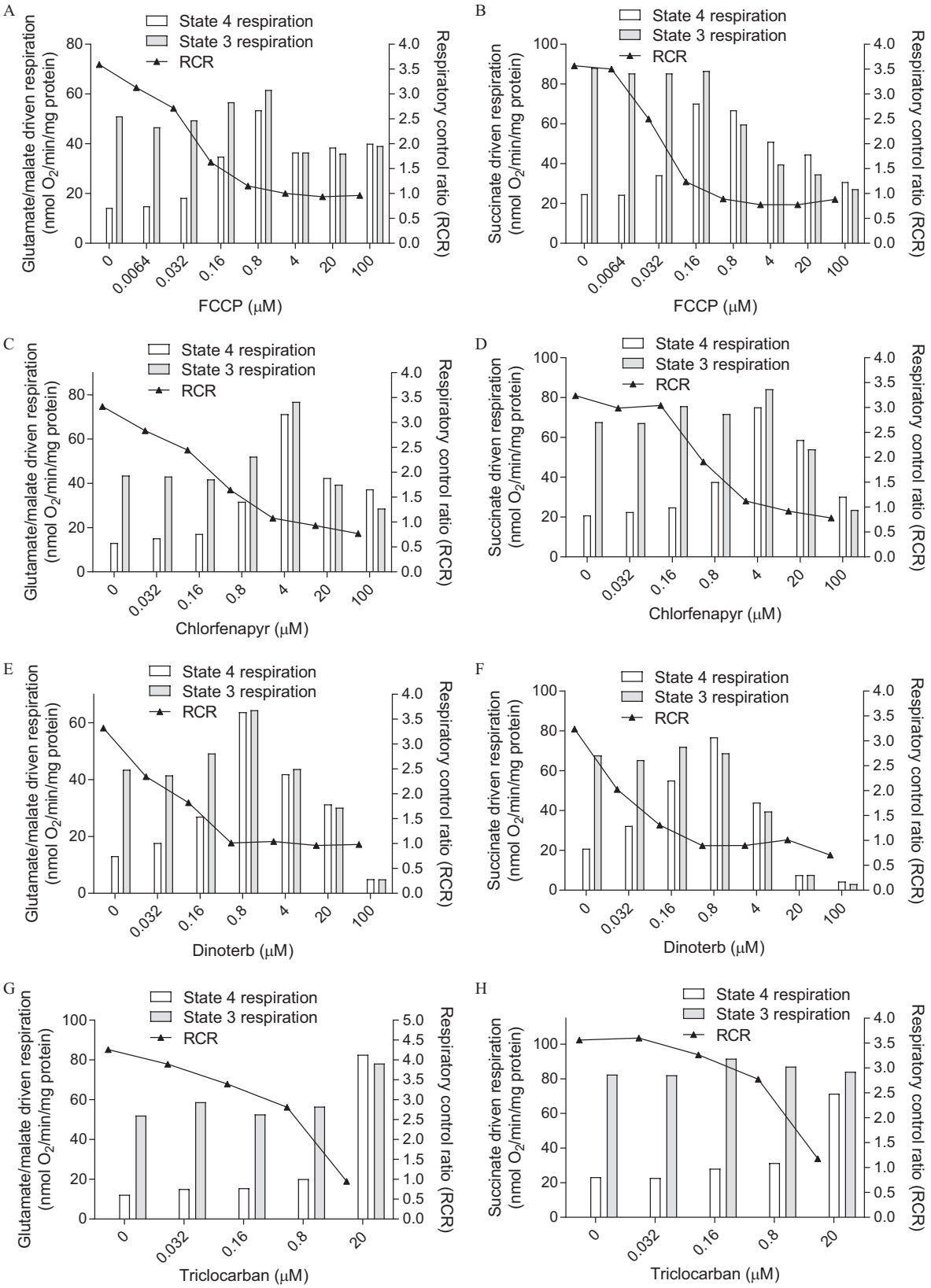

Figure 2. Mitochondrial oxygen consumption and respiratory control ratios for representative compounds exhibiting effects similar to uncouplers of mitochondrial respiration. Oxygen consumption was measured using the Clark-type oxygen electrode after isolated rat liver mitochondria were incubated with various concentrations of (*A* and *B*) FCCP, (*C* and *D*) chlorfenapyr, (*E* and *F*) dinoterb, and (*G* and *H*) triclocarban. FCCP, carbonyl cyanide 4-(trifluoromethoxy)phenylhydrazone; RCR, respiratory control ratio. The bars represent oxygen consumption rate and the line indicates respiratory control ratio. Data are from one experiment.

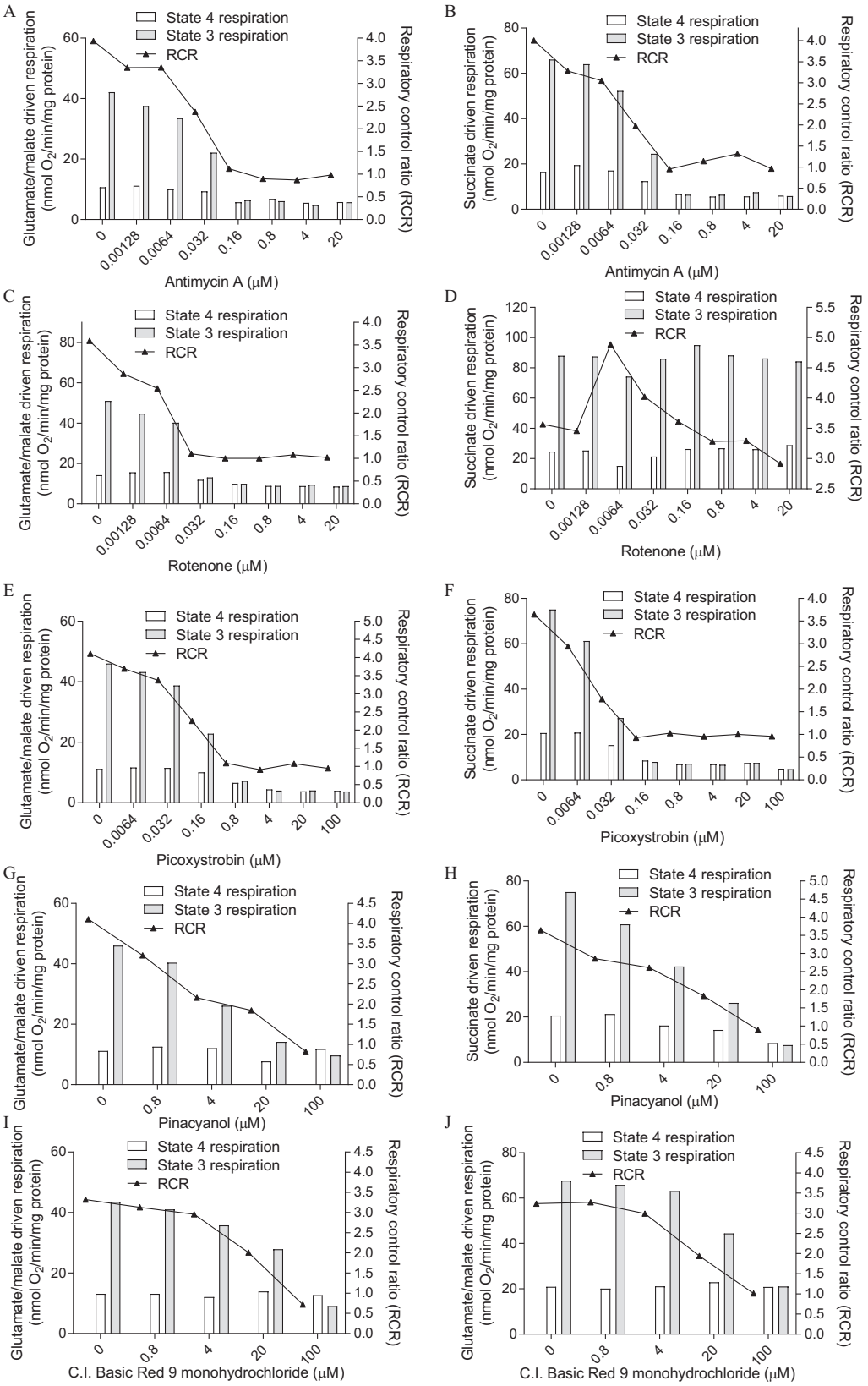

Figure 3. Mitochondrial oxygen consumption and respiratory control ratios for compounds exhibiting effects similar to inhibitors of mitochondrial respiration. Oxygen consumption was measured using the Clark-type oxygen electrode after the isolated rat liver mitochondria were incubated with various concentrations of (*A* and *B*) antimycin A, (*C* and *D*) rotenone, (*E* and *F*) picoxystrobin, (*G* and *H* pinacyanol, and (*I* and *J*) C.I. Basic Red 9 monohydrochloride. The bars represent oxygen consumption rate and the line indicates respiratory control ratio (RCR). Data are from one experiment.

Table 3. Effect of compounds on oxygen consumption in HepG2 cells using the Seahorse method and Parkin translocation in HeLa cells expressing YFP-Parkin.

Compound	CASRN	Activity in oxygen consumption[a]	Parkin recruitment[b]
1,4-Diaminoanthraquinone	128–95–0	Inactive	Inactive
1,8-Dihydroxy-4,5-dinitroanthraquinone	81–55–0	Uncoupler + inhibitor	Inactive
2,2′-Methylenebis(4-methyl-6-*tert*-butylphenol)	119–47–1	Uncoupler	Inactive
2,2′-Methylenebis(ethyl-6-*tert*-butylphenol)	88–24–4	Uncoupler	Inactive
2-Aminoanthraquinone	117–79–3	Inactive	Inactive
2-Hydrazino-4-(4-aminophenyl) thiazole	26049–71–8	Inactive	Inactive
2-Hydrazino-4-(4-nitrophenyl)thiazole	26049–70–7	Inactive	Active
2-Hydrazino-4-phenylthiazole	34176–52–8	Inactive	Inactive
5HPP-33	105624–86–0	Uncoupler + inhibitor	Active
Antimycin A	1397–94–0	Inhibitor	Active
Bexarotene	153559–49–0	Uncoupler + inhibitor	Inactive
C.I. Basic Red 9 monohydrochloride	569–61–9	Inhibitor	Inactive
Chlorfenapyr	122453–73–0	Uncoupler + inhibitor	Active
Chlorophacinone	3691–35–8	Uncoupler + inhibitor	Inactive
Diclazuril	101831–37–2	Uncoupler + inhibitor	Inactive
Dinoseb	88–85–7	Uncoupler + inhibitor	Active
Dinoterb	1420–07–1	Uncoupler + inhibitor	Active
Diphenylurea	102–07–8	Inactive	Inactive
Emodin	518–82–1	Uncoupler	Active
Lasalocid sodium	25999–20–6	Uncoupler + inhibitor	Inactive
Niclosamide	50–65–7	Uncoupler + inhibitor	Active
Niflumic acid	4394–00–7	Uncoupler	Inactive
Palmatine chloride hydrate	171869–95–7	Inactive	Inactive
FCCP	370–86–5	Uncoupler + inhibitor	Active
Picoxystrobin	117428–22–5	Inhibitor	Inactive
Pinacyanol	605–91–4	Inhibitor	Active
Rafoxanide	22662–39–1	Uncoupler + inhibitor	Active
Rhein	478–43–3	Uncoupler	Inactive
Rifampicin	13292–46–1	Inactive	Inactive
Rifapentine	61379–65–5	Inhibitor	Inactive
Rotenone	83–79–4	Inhibitor	Inactive
Thidiazuron	51707–55–2	Inactive	Inactive
Triclocarban	101–20–2	Uncoupler	Active
Triethyltin bromide	2767–54–6	Uncoupler + inhibitor	Inactive

[a]Measurement of intact cellular respiration was performed using the Seahorse XF24 analyzer with 25 mM glucose as the extracellular substrate. Respiration was measured under the basal condition and in the presence of each compound at four concentrations to assess oxidative capacity. If a compound caused significant increases in oxygen consumption rate compared with basal condition, it was considered as an uncoupler. If a compound caused a significant decreased in oxygen consumption rate compared with basal condition, it was considered as an inhibitor. As described in the Clark-type oxygen electrode assay, a compound can be an uncoupler as lower concentration, and an inhibitor at higher concentration. If a compound did not significantly affect oxygen consumption rate at tested concentrations, then it was considered as inactive.
[b]Parkin translocation assay was performed using a HeLa cell line stably expressing YFP-Parkin. These cells were treated for 2 h with DMSO as vehicle control or with tested compounds at indicated concentrations. Fluorescent samples of YFP-Parkin were examined with a Zeiss LSM 780 confocal microscope, and active was determined when YFP-Parkin was recruited to mitochondria upon compound treatment as shown in Figure 6.

to affect (*a*) larval development and growth as measured by extinction (EXT) or size of individual nematodes, and (*b*) mitochondrial toxicity through ATP content as measured by luminescence of a transgenic nematode strain expressing luciferase. Five chemicals of 34 (chlorfenapyr, pinacyanol, rotenone, triclocarban, and triethyltin bromide) led to severe larval growth arrest at 0.5 μM and were tested at additional lower concentrations. Compound activity was assessed by calculating the lowest effect concentration (LEC) for each assay across all concentrations tested.

Of the 34 compounds tested in *C. elegans*, 24 inhibited larval growth and decreased ATP content. The 10 most potent compounds had LECs <10 μM for both assays including those 5 compounds listed above that required testing at lower concentrations, along with chlorophacinone, diclazuril, FCCP, dinoterb, and picoxystrobin (see Excel Table S3 and Figure S3). Four synthetic dyes had LECs ≤ 10 μM for the ATP assay but lower potency in the larval growth assay (2-aminoanthraquinone, 1,4-diaminoanthraquinone, C.I. Basic Red 9 monohydrochloride, and 1,8-dihydroxy-4,5-dinitroanthraquinone). These 14 chemicals are most likely to be potent *in vivo* mitotoxicants per the *C. elegans* data (see orange shading in Excel Table S3).

Six additional chemicals (rafoxanide, lasalocid sodium, 2,2′-methylenebis(4-methyl-6-*tert*-butylphenol, 2,2′-methylenebis(ethyl-6-*tert*-butylphenol), 2-hydrazino-4-phenylthiazole, and bexarotene) had LECs ≤ 10 μM for the larval growth assay with lower potency or inactivity in the ATP assay, which is suggestive of general toxicity. Five chemicals caused statistically significant decreases in ATP content and did not affect growth across the tested concentrations (diphenylurea, emodin, thiadiazuron, niflumic acid, and rifapentine). Although statistically significant, the decreases in ATP may not be biologically relevant given that they did not lead to observations of retarded larval growth. The remaining four chemicals showed no activity in either assay (see gray shading in Excel Table S3).

Discussion

In the current study, we used a tiered testing strategy (Figure 1) to evaluate and prioritize chemicals for potential mitochondrial toxicity, as detected initially by a large-scale, concentration–response screen (Attene-Ramos et al. 2015), for further in-depth investigation with a variety of mechanistic assays. Previously well-characterized mitochondrial toxicants including FCCP and rotenone were among the most active compounds in these mechanistic assays. The 10 most active chemicals (based on the lowest IC_{50} values or concentrations) were chlorfenapyr ($IC_{50} = 0.31$ μM in the hNSC MMP assay, uncoupler effect at 0.16 μM in the oxygen consumption assay, and inhibitory effect at 0.05 and 0.25 μM on larval growth and ATP content in the *C. elegans* assays, respectively); dinoterb

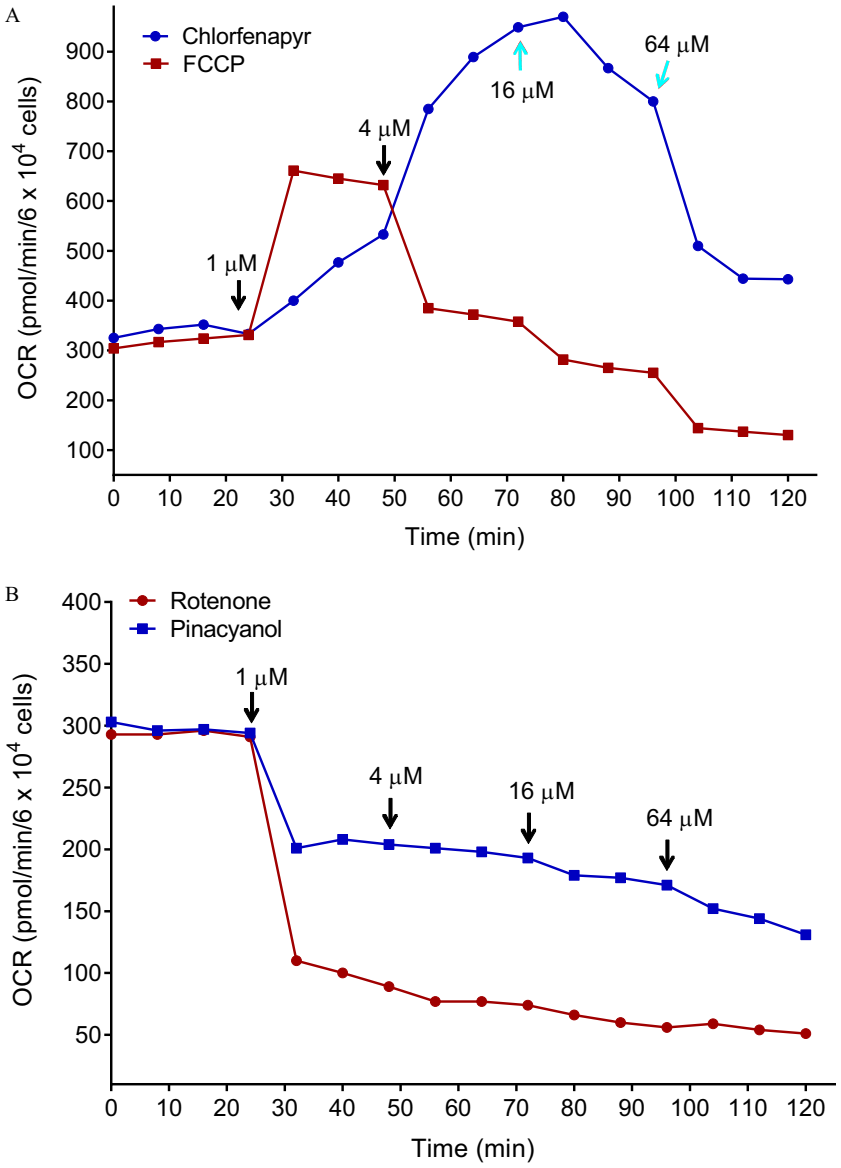

Figure 4. Confirmation of the effect of representative mitochondrial uncouplers and inhibitors on mitochondrial respiration. The rate of oxygen consumption was measured using a Seahorse XF24 analyzer in the HepG2 cells before and after treatment with various concentrations of (*A*) FCCP and chlorfenapyr, and (*B*) rotenone and pinacyanol. FCCP, carbonyl cyanide 4-(trifluoromethoxy)phenylhydrazone. Representative curves are from one of three experiments.

(uncoupler effect at 0.032 μM in the oxygen consumption assay, $EC_{50} = 0.52$ μM in the ARE assay, and inhibitory effect at 1.0 μM on ATP content in the *C. elegans* assay); lasalocid ($IC_{50} = 0.54$ μM in the hNSC MMP assay); picoxystrobin ($IC_{50} = 0.75$ μM in the ARE assay and inhibitory effect on Complex III at 4 μM); pinacyanol ($IC_{50} = 0.04$ μM in both the HepG2 and hNSC MMP assays; 23.6% inhibition effect on Complex I at 4.0 μM, and an inhibitory effect at 0.005 μM on larval growth in the *C. elegans* assay); triclocarban ($IC_{50} = 0.43$ μM in the hNSC MMP assay); and triethyltin bromide ($IC_{50} = 0.65$ μM in the HepG2 MMP assay, uncoupler effect at 0.8 μM in the oxygen consumption assay) as well as the well-known mitochondria toxicants antimycin A (inhibitory effect on Complex III at 0.032 μM), FCCP (uncoupler effect at 0.032 μM in the oxygen consumption assay and $IC_{50} = 0.27$ μM in the hNSC MMP assay), and rotenone (inhibitory effect on Complex I at 0.032 μM and inhibitory effect at 0.05 μM on larval growth in the *C. elegans* assay). Among these 10 most active compounds, 4—lasalocid, picoxystrobin, pinacyanol, and triclocarban—have not been well characterized previously to be mitochondria toxicants. Thus, these results illustrate the value of using a battery of assays to identify mitochondrial toxicants.

Species- or cell type-specific sensitivity to some compounds was observed in the present study. For example, the pesticide rotenone was much more potent in rat hepatocytes ($IC_{50} = 0.36$ μM) compared with hNSC ($IC_{50} = 23.7$ μM) and HepG2 cells ($IC_{50} =$ 44.7 μM). Rotenone is known to inhibit complex I of the electron transport chain. Rats exposed to rotenone developed the features of Parkinson disease (PD) through complex I inhibition leading to selective degeneration of the nigrostriatal dopaminergic neurons (Betarbet et al. 2000; Sherer et al. 2003). Furthermore, there is an increasing risk of PD with chronic exposure to pesticides (Nandipati and Litvan 2016; Priyadarshi et al. 2000), but there is no clear evidence for a direct link between rotenone use in agricultural applications and PD development in humans (Nandipati and Litvan 2016). The low sensitivity of HepG2 cells to rotenone in the MMP assay may be related to the significant activation of the Nrf2/ARE pathway by rotenone ($EC_{50} = 50$ nM) given that Nrf2 is a transcription factor that regulates important antioxidant and

Table 4. Compound inhibition [percentage (%)] on mitochondrial respiratory chain complex I–V in isolated rat liver mitochondria.

Compound	Complex I % inhibition	Complex II % inhibition	Complex III % inhibition	Complex IV % inhibition	Complex V % inhibition
2-Hydrazino-4-(4-nitrophenyl)thiazole	21.6 ± 7.1 at 100 μM	Inactive	Inactive	Inactive	Inactive
Antimycin A	Inactive	Inactive	71.1 ± 2.91 at 0.032 μM	Inactive	Inactive
Bexarotene	Inactive	Inactive	Inactive	Inactive	Inactive
C.I. Basic Red 9 monohydrochloride	14.1 ± 2.98 at 100 μM	12.2 ± 3.48 at 100 μM	21.6 ± 6.41 at 100 μM	Inactive	Inactive
Lasalocid sodium	18.3 ± 6.97 at 100 μM	Inactive	Inactive	Inactive	Inactive
Palmatine chloride hydrate	12.3 ± 3.05 at 100 μM	Inactive	Inactive	Inactive	Inactive
Picoxystrobin	13.2 ± 3.23 at 20 μM	Inactive	53.3 ± 3.26 at 4 μM	Inactive	Inactive
Pinacyanol	38.3 ± 1.92 at 20 μM	Inactive	Inactive	Inactive	Inactive
Rafoxanide	Inactive	44.4 ± 6.56 at 0.8 μM	Inactive	Inactive	40.1 ± 1.87 at 20 μM
Rotenone	37.5 ± 3.32 at 0.032 μM	Inactive	Inactive	Inactive	Inactive
Triethyltin bromide	Inactive	Inactive	Inactive	Inactive	57.4 ± 3.74 at 20 μM

Note: Each compound was tested starting at 100 μM. If there was statistically significant inhibition compared with DMSO control, then next concentration of compound (i.e., 20, 4, 0.8, 016, 0.032, 0.0064, and 0.00128 μM) would be tested until there was no inhibition observed. The % inhibition was determined using 100% minus the activities from DMSO control. The value of % inhibition of compound is the mean ± SD of the results from three experiments. The compound with no activity detected up to 100 μM was defined as inactive. Data listed in the table represent the lowest concentration that caused inhibition or the concentration that caused >35% inhibition.

phase II detoxification enzymes (Todorovic et al. 2016). As previously reported (Siddiqui et al. 2013), we also found that rotenone, after a 24-h treatment, induced cytotoxicity in HepG2 cells that may be linked to increased ROS level and activation of p53 signaling. The underlying mechanism of these rotenone effects still needs further investigation. In addition, from the current study, the low glucose (5 mM) condition seems not to affect IC_{50} values when compared with the galactose condition. Different IC_{50} values were commonly observed between experiments that used galactose and high (25 mM) glucose concentrations (Marroquin et al. 2007).

Mitochondria dysfunction has been linked to overproduction of ROS in mitochondria (Bai and Cederbaum 2001), activation of cellular signaling pathways including Nrf2/ARE pathway (Miller et al. 2013), and p53 signaling (Villeneuve et al. 2013). Mitochondrial damage can also be recognized by the protein phosphatase and tensin homolog (PTEN)-induced kinase 1 (PINK1), which recruits Parkin to the mitochondrial outer membrane to initiate Parkin-mediated autophagy (mitophagy) (Narendra et al. 2008). Both of these proteins are genetically linked to PD (Pickrell and Youle 2015; Zheng and Hunter 2013). Among the 34 compounds tested, we found that 22 (65%) induced ROS and 24 (71%) activated the

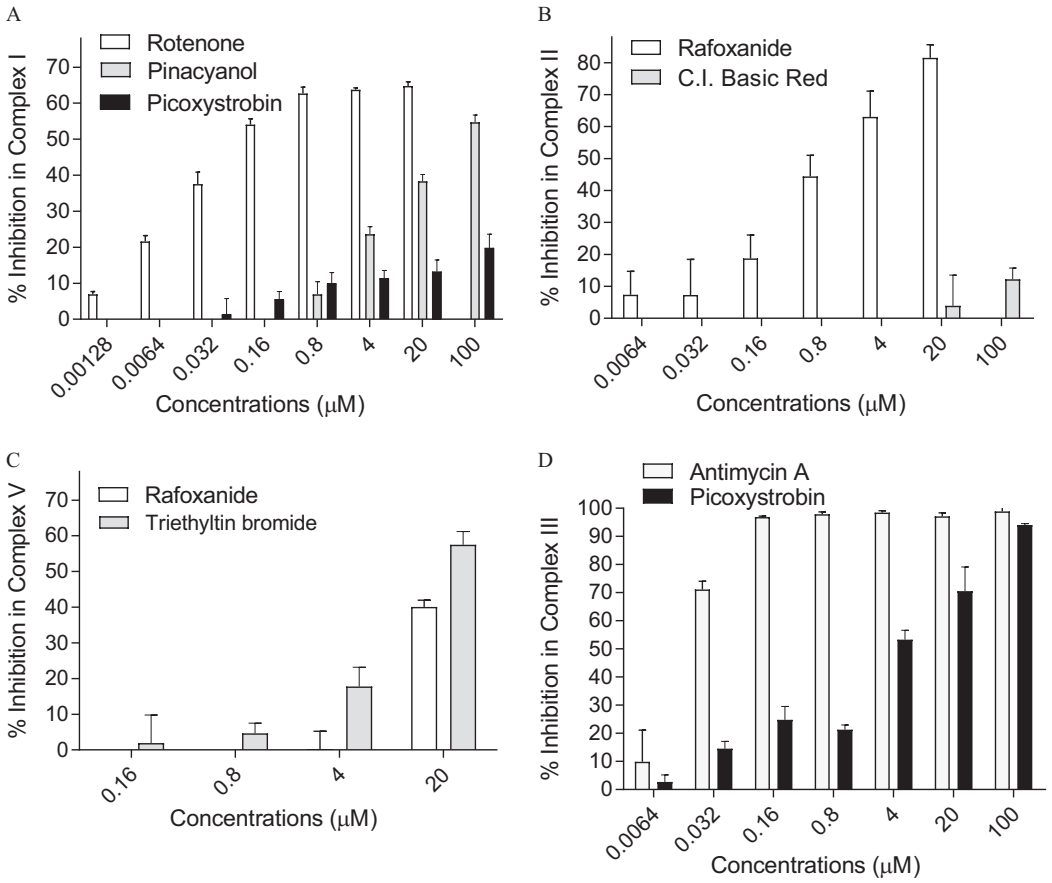

Figure 5. Effect of representative compounds on the activity of mitochondrial complexes (*A*) 1, (*B*) II, (*C*) V, and (*D*) III. Submitochondrial particles were isolated from rat liver and the activities of the respiratory complex chain complexes were measured biochemically. Percentage inhibition was determined by 100% minus the percentage of DMSO control. FCCP, carbonyl cyamide 4-(trifluoromethoxy)phenylhydrazone. Data represent mean ± SD from three experiments.

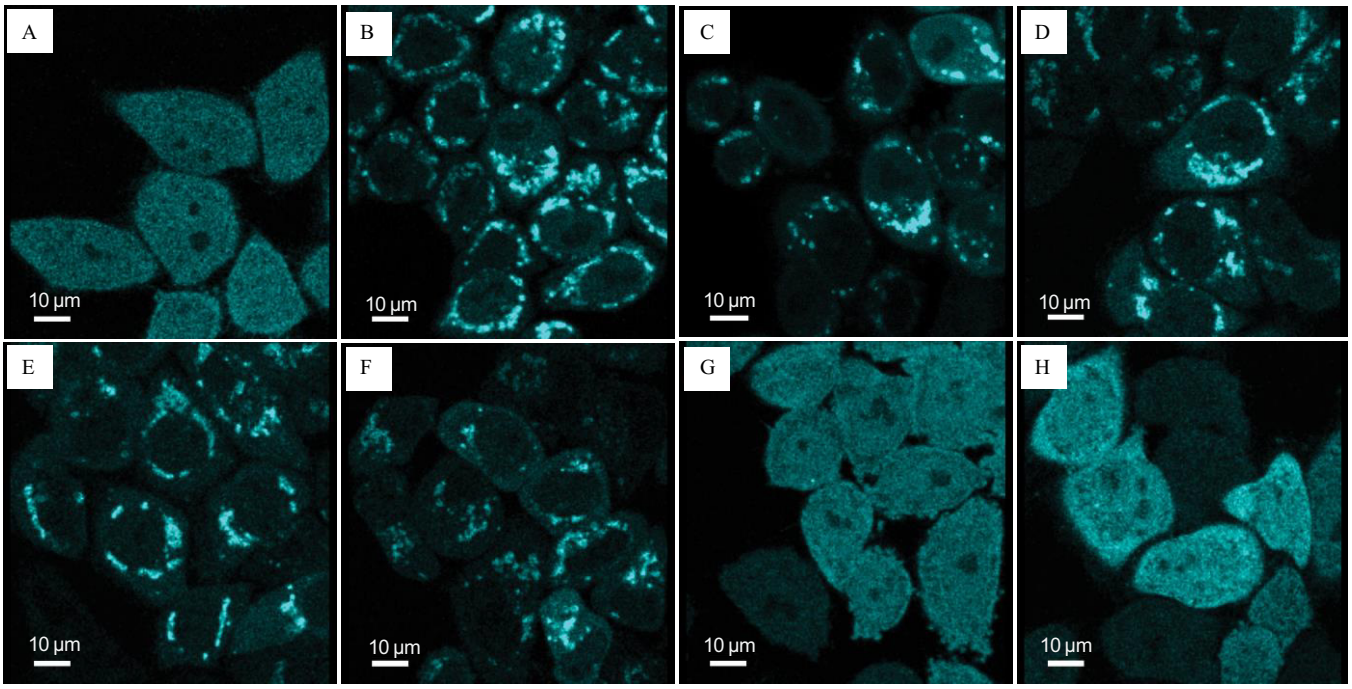

Figure 6. Effect of compounds on Parkin translocation in YFP-engineered HeLa cells. After treatment with (*A*) dimethylsulfoxide (DMSO) only, (*B*) carbonyl cyanide 4-(trifluoromethoxy)phenylhydrazone (FCCP, 10 μM), (*C*) antimycin A (10 μM), (*D*) chlorfenapyr (16 μM), (*E*) dinoterb (64 μM), (*F*) pinacyanol (4 μM), (*G*) rotenone (16 μM), and (*H*) picoxystrobin (16 μM) for 3 h, recruitment of Parkin to mitochondria was measured in YFP-expressing HeLa cells. FCCP, carbonyl cyamide 4-(trifluoromethoxy)phenylhydrazone. Representative confocal images were acquired in a Zeiss LSM 780 confocal microscope using a 40× oil objective.

Nrf2/ARE pathway, whereas 14 (41%) activated p53 signaling and 12 (35%) induced Parkin translocation. However, there was not a strong correlation in compound potencies between the ROS and Nrf2/ARE assays. This may be due to different mechanisms of compound action detected in these two assays, each of which measures some aspect of oxidative damage. Investigation of mechanisms of action is a key step in the prioritization of chemicals for more extensive toxicological assessment. Pinacyanol, a cyanine dye, was identified from the current study as a mitochondrial toxin with a mechanism of action similar to rotenone (i.e., complex I inhibition). Although pinacyanol has diverse applications in synthetic, analytical, and industrial fields (Ganguly and Prasad 2012), its toxicity has not been extensively studied.

There is growing a recognition that environmental factors may be linked to neurodegeneration risk (Pearson et al. 2016). Recent research indicated that several inhibitors of the electron transport chain can induce parkinsonism-like symptoms in rats (Winklhofer and Haass 2010). Upon mitochondrial damage, the E3 ubiquitin ligase, Parkin, is recruited to damaged mitochondria by PINK1 (Narendra et al. 2008) to induce mitophagy. We found that FCCP, antimycin A, and pinacyanol can activate this PINK1/Parkin pathway, consistent with their roles in causing mitochondria damage. We also observed that higher concentrations of FCCP decreased state 3 respiration and reduced the extent of the increases in state 4 respiration. This suggests that FCCP also inhibits respiration at higher concentrations. However, some of the compounds, such as rotenone and picoxystrobin, which have been identified as mitochondria toxicants, did not induce Parkin translocation to mitochondria. Previous studies demonstrated that rotenone was not able to increase PINK1 levels or induce Parkin translocation to mitochondria (Chu et al. 2013). Picoxystrobin, a fungicide belonging to the strobilurin group of chemicals, is used for control of fungal diseases of agriculture products and is the top-selling fungicide-active substance in the world with sales exceeding $1 billion (Uttley 2011). These chemicals have been identified as risk factors of various brain disorders (Pearson et al. 2016). Picoxystrobin's fungicidal activity is mediated through the inhibition of agricultural soil microbial respiration activity (Stenrød et al. 2013). In the present study, we found that picoxystrobin decreased MMP and inhibited cellular respiration by blocking mitochondrial electron transport at complex III. Picoxystrobin also increased the production of ROS, and induced p53 and ARE signaling, which may be the direct consequences of mitochondrial dysfunction.

Reducing the use of mammals in toxicity testing is one of the goals of chemical prioritization as informed by *in vitro* assays. To assess whether the *in vitro* assays employed here model *in vivo* effects, the 34 compounds were tested for effects on larval development and ATP content in the nematode *C. elegans*. Most of the compounds (28/34, 82%) that were active in the *in vitro* MMP assays were also active in the *C. elegans* assays, suggesting that *C. elegans* models are useful tools for screening compounds before further testing in mammalian models. The four novel compounds—pinacyanol, lasalocid, picoxystrobin and triclocarban—identified in the current study as candidates for further testing, all inhibited mitochondrial ATP levels and larval development/growth, confirming previous findings that mitochondrial toxicants retard larval development in *C. elegans* (Behl et al. 2016; Bess et al. 2012). Recently, Bhhatarai et al. (2015) reported that the data generated in the *in vitro* MMP assay directly correlated with data obtained in *in vivo* toxicity studies in fish, *Daphnia*, and rats dosed by the intravenous route, but not the oral route. Oral administration of the compounds may alter the acute toxicity of compounds in mammals due to the first pass liver effect, bioavailability, and metabolism. Therefore, these novel mitochondrial toxicants should be further evaluated for their ability to potentially cause adverse health effects in humans.

In summary, our study provides a strategy based on a tiered testing approach that can be used to prioritize a large set of environmental chemicals for testing for mitochondrial toxicity. The mitochondrial toxicants identified in our study using this approach should be considered high priority candidates for potential toxicity assessment. A similar systematic prioritization strategy could also be applied to other cellular targets and pathways in an effort to reduce animal use while efficiently identifying toxicants and generating useful mechanistic information applicable to the understanding of human exposure risk.

Acknowledgments

We thank R. Youle (National Institute of Neurological Disorders and Stroke/NIH) for providing the Parkin-overexpressing HeLa cell line. This work was supported by the U.S. Environmental Protection Agency (EPA; Interagency Agreement #Y3-HG-7026-03), the National Center for Advancing Translational Sciences (NCATS) Intramural Research Program, and the National Institutes of Health's National Institute of Environmental Health Sciences/Division of the National Toxicology Program to the NCATS (Interagency Agreement IAA #NTR 12003).

The views expressed in this paper are those of the authors and do not necessarily reflect the statements, opinions, views, conclusions, or policies of the Environmental Protection Agency, the National Institute of Environmental Health Sciences, the National Center for Advancing Translational Sciences, National Institutes of Health, the Food and Drug Administration, or the United States government. Mention of trade names or commercial products does not constitute endorsement or recommendation for use.

References

Attene-Ramos MS, Huang R, Michael S, Witt KL, Richard A, Tice RR, et al. 2015. Profiling of the Tox21 chemical collection for mitochondrial function to identify compounds that acutely decrease mitochondrial membrane potential. Environ Health Perspect 123(1):49–56, PMID: 25302578, https://doi.org/10.1289/ehp.1408642.

Attene-Ramos MS, Huang R, Sakamuru S, Witt KL, Beeson GC, Shou L, et al. 2013. Systematic study of mitochondrial toxicity of environmental chemicals using quantitative high throughput screening. Chem Res Toxicol 26(9):1323–1332, PMID: 23895456, https://doi.org/10.1021/tx4001754.

Bai J, Cederbaum AI. 2001. Mitochondrial catalase and oxidative injury. Biol Signals Recept 10(3–4):189–199, PMID: 11351128, https://doi.org/10.1159/000046887.

Behl M, Rice JR, Smith MV, Co CA, Bridge MF, Hsieh J-H, et al. 2016. Editor's highlight: comparative toxicity of organophosphate flame retardants and polybrominated diphenyl ethers to *Caenorhabditis elegans*. Toxicol Sci 154(2):241–252, PMID: 27566445, https://doi.org/10.1093/toxsci/kfw162.

Bess AS, Crocker TL, Ryde IT, Meyer JN. 2012. Mitochondrial dynamics and autophagy aid in removal of persistent mitochondrial DNA damage in *Caenorhabditis elegans*. Nucleic Acids Res 40(16):7916–7931, PMID: 22718972, https://doi.org/10.1093/nar/gks532.

Betarbet R, Sherer TB, MacKenzie G, Garcia-Osuna M, Panov AV, Greenamyre JT. 2000. Chronic systemic pesticide exposure reproduces features of Parkinson's disease. Nat Neurosci 3(12):1301–1306, PMID: 11100151, https://doi.org/10.1038/81834.

Bhhatarai B, Wilson DM, Bartels MJ, Chaudhuri S, Price PS, Carney EW. 2015. Acute toxicity prediction in multiple species by leveraging mechanistic ToxCast mitochondrial inhibition data and simulation of oral bioavailability. Toxicol Sci 147(2):386–396, PMID: 26139166, https://doi.org/10.1093/toxsci/kfv135.

Boyd WA, Smith MV, Co CA, Pirone JR, Rice JR, Shockley KR. 2016. Developmental effects of the ToxCast™ Phase I and Phase II chemicals in *Caenorhabditis elegans* and corresponding responses in zebrafish, rats, and rabbits. Environ Health Perspect 124(5):586–593, PMID: 26496690, https://doi.org/10.1289/ehp.1409645.

Boyd WA, Smith MV, Kissling GE, Freedman JH. 2010. Medium- and high-throughput screening of neurotoxicants using *C. elegans*. Neurotoxicol Teratol 32(1):68–73, PMID: 19166924, https://doi.org/10.1016/j.ntt.2008.12.004.

Boyd WA, Smith MV, Kissling GE, Rice JR, Snyder DW, Portier CJ, et al. 2009. Application of a mathematical model to describe the effects of chlorpyrifos on *Caenorhabditis elegans* development. PLoS One 4(9):e7024, PMID: 19753116, https://doi.org/10.1371/journal.pone.0007024.

Chen S, Hsieh J-H, Huang R, Sakamuru S, Hsin L-Y, Xia M, et al. 2015. Cell-based high-throughput screening for aromatase inhibitors in the Tox21 10K library. Toxicol Sci 147(2):446–457, PMID: 26141389, https://doi.org/10.1093/toxsci/kfv141.

Chu CT, Ji J, Dagda RK, Jiang JF, Tyurina YY, Kapralov AA, et al. 2013. Cardiolipin externalization to the outer mitochondrial membrane acts as an elimination signal for mitophagy in neuronal cells. Nat Cell Biol 15(10):1197–1205, PMID: 24036476, https://doi.org/10.1038/ncb2837.

Dinkova-Kostova AT, Abramov AY. 2015. The emerging role of Nrf2 in mitochondrial function. Free Radic Biol Med 88(pt B):179–188, PMID: 25975984, https://doi.org/10.1016/j.freeradbiomed.2015.04.036.

Dix DJ, Houck KA, Martin MT, Richard AM, Setzer RW, Kavlock RJ. 2007. The ToxCast program for prioritizing toxicity testing of environmental chemicals. Toxicol Sci 95(1):5–12, PMID: 16963515, https://doi.org/10.1093/toxsci/kfl103.

Ganguly B, Prasad S. 2012. Homology modeling and functional annotation of bubaline pregnancy associated glycoprotein 2. J Anim Sci Biotechnol 3(1):13, PMID: 22958467, https://doi.org/10.1186/2049-1891-3-13.

Hsu C-W, Zhao J, Huang R, Hsieh J-H, Hamm J, Chang X, et al. 2014. Quantitative high-throughput profiling of environmental chemicals and drugs that modulate farnesoid X receptor. Sci Rep 4:6437, PMID: 25257666, https://doi.org/10.1038/srep06437.

Huang R. 2016. A quantitative high-throughput screening data analysis pipeline for activity profiling. Methods Mol Biol 1473:111–122, PMID: 27518629, https://doi.org/10.1007/978-1-4939-6346-1_12.

Huang R, Sakamuru S, Martin MT, Reif DM, Judson RS, Houck KA, et al. 2014. Profiling of the Tox21 10K compound library for agonists and antagonists of the estrogen receptor alpha signaling pathway. Sci Rep 4:5664, PMID: 25012808, https://doi.org/10.1038/srep05664.

Huang R, Xia M, Sakamuru S, Zhao J, Shahane SA, Attene-Ramos M, et al. 2016. Modelling the Tox21 10 K chemical profiles for *in vivo* toxicity prediction and mechanism characterization. Nat Commun 7:10425, PMID: 26811972, https://doi.org/10.1038/ncomms10425.

Judson RS, Magpantay FM, Chickarmane V, Haskell C, Tania N, Taylor J, et al. 2015. Integrated model of chemical perturbations of a biological pathway using 18 *in vitro* high-throughput screening assays for the estrogen receptor. Toxicol Sci 148(1):137–154, PMID: 26272952, https://doi.org/10.1093/toxsci/kfv168.

Kavlock RJ, Austin CP, Tice RR. 2009. Toxicity testing in the 21st century: implications for human health risk assessment. Risk Anal 29(4):485–487, PMID: 19076321, https://doi.org/10.1111/j.1539-6924.2008.01168.x.

Kirby DM, Thorburn DR, Turnbull DM, Taylor RW. 2007. Biochemical assays of respiratory chain complex activity. Methods Cell Biol 80:93–119, PMID: 17445690, https://doi.org/10.1016/S0091-679X(06)80004-X.

Kohonen T. 2006. Self-organizing neural projections. Neural Netw 19(6–7):723–733, PMID: 16774731, https://doi.org/10.1016/j.neunet.2006.05.001.

Lagido C, McLaggan D, Flett A, Pettitt J, Glover LA. 2009. Rapid sublethal toxicity assessment using bioluminescent *Caenorhabditis elegans*, a novel whole-animal metabolic biosensor. Toxicol Sci 109(1):88–95, PMID: 19299418, https://doi.org/10.1093/toxsci/kfp058.

Lenaz G, Bovina C, D'Aurelio M, Fato R, Formiggini G, Genova ML, et al. 2002. Role of mitochondria in oxidative stress and aging. Ann N Y Acad Sci 959:199–213, PMID: 11976197, https://doi.org/10.1111/j.1749-6632.2002.tb02094.x.

Mammucari C, Rizzuto R. 2010. Signaling pathways in mitochondrial dysfunction and aging. Mech Ageing Dev 131(7–8):536–543, PMID: 20655326, https://doi.org/10.1016/j.mad.2010.07.003.

Marchetti P, Castedo M, Susin SA, Zamzami N, Hirsch T, Macho A, et al. 1996. Mitochondrial permeability transition is a central coordinating event of apoptosis. J Exp Med 184(3):1155–1160, PMID: 9064332, https://doi.org/10.1084/jem.184.3.1155.

Marroquin LD, Hynes J, Dykens JA, Jamieson JD, Will Y. 2007. Circumventing the Crabtree effect: replacing media glucose with galactose increases susceptibility of HepG2 cells to mitochondrial toxicants. Toxicol Sci 97(2):539–547, PMID: 17361016, https://doi.org/10.1093/toxsci/kfm052.

Miller DM, Singh IN, Wang JA, Hall ED. 2013. Administration of the Nrf2-ARE activators sulforaphane and carnosic acid attenuates 4-hydroxy-2-nonenal-induced mitochondrial dysfunction ex vivo. Free Radic Biol Med 57:1–9, PMID: 23275005, https://doi.org/10.1016/j.freeradbiomed.2012.12.011.

Nandipati S, Litvan I. 2016. Environmental exposures and Parkinson's disease. Int J Environ Res Public Health 13(9):881, https://doi.org/10.3390/ijerph13090881.

Narendra D, Tanaka A, Suen D-F, Youle RJ. 2008. Parkin is recruited selectively to impaired mitochondria and promotes their autophagy. J Cell Biol 183(5):795–803, PMID: 19029340, https://doi.org/10.1083/jcb.200809125.

Nezich CL, Wang C, Fogel AI, Youle RJ. 2015. MIT/TFE transcription factors are activated during mitophagy downstream of Parkin and Atg5. J Cell Biol 210(3):435–450, PMID: 26240184, https://doi.org/10.1083/jcb.201501002.

NIEHS (National Institute of Environmental Health Sciences). 2017. The New Environmental Health: How You'll Live Longer, Smarter. https://www.niehs.nih.gov/health/materials/new_environmental_health_the_508.pdf [accessed 15 February 2017].

Pearson BL, Simon JM, McCoy ES, Salazar G, Fragola G, Zylka MJ. 2016. Identification of chemicals that mimic transcriptional changes associated with autism, brain aging and neurodegeneration. Nat Commun 7:11173, PMID: 27029645, https://doi.org/10.1038/ncomms11173.

Pickrell AM, Youle RJ. 2015. The roles of PINK1, Parkin, and mitochondrial fidelity in Parkinson's disease. Neuron 85(2):257–273, PMID: 25611507, https://doi.org/10.1016/j.neuron.2014.12.007.

Priyadarshi A, Khuder SA, Schaub EA, Shrivastava S. 2000. A meta-analysis of Parkinson's disease and exposure to pesticides. Neurotoxicology 21(4):435–440, PMID: 11022853.

Ravagnan L, Roumier T, Kroemer G. 2002. Mitochondria, the killer organelles and their weapons. J Cell Physiol 192(2):131–137, PMID: 12115719, https://doi.org/10.1002/jcp.10111.

Rotroff DM, Martin MT, Dix DJ, Filer DL, Houck KA, Knudsen TB, et al. 2014. Predictive endocrine testing in the 21st century using in vitro assays of estrogen receptor signaling responses. Environ Sci Technol 48(15):8706–8716, PMID: 24960280, https://doi.org/10.1021/es502676e.

Sakamuru S, Li X, Attene-Ramos MS, Huang R, Lu J, Shou L, et al. 2012. Application of a homogenous membrane potential assay to assess mitochondrial function. Physiol Genomics 44(9):495–503, PMID: 22433785, https://doi.org/10.1152/physiolgenomics.00161.2011.

Shaughnessy DT, McAllister K, Worth L, Haugen AC, Meyer JN, Domann FE, et al. 2014. Mitochondria, energetics, epigenetics, and cellular responses to stress. Environ Health Perspect 122(12):1271–1278, PMID: 25127496, https://doi.org/10.1289/ehp.1408418.

Sherer TB, Betarbet R, Testa CM, Seo BB, Richardson JR, Kim JH, et al. 2003. Mechanism of toxicity in rotenone models of Parkinson's disease. J Neurosci 23(34):10756–10764, PMID: 14645467, https://doi.org/10.1523/JNEUROSCI.23-34-10756.2003.

Shukla SJ, Huang R, Austin CP, Xia M. 2010. The future of toxicity testing: a focus on *in vitro* methods using a quantitative high-throughput screening platform. Drug Discov Today 15(23–24):997–1007, PMID: 20708096, https://doi.org/10.1016/j.drudis.2010.07.007.

Siddiqui MA, Ahmad J, Farshori NN, Saquib Q, Jahan S, Kashyap MP, et al. 2013. Rotenone-induced oxidative stress and apoptosis in human liver HepG2 cells. Mol Cell Biochem 384(1–2):59–69, PMID: 23963993, https://doi.org/10.1007/s11010-013-1781-9.

Smith MV, Boyd WA, Kissling GE, Rice JR, Snyder DW, Portier CJ, et al. 2009. A discrete time model for the analysis of medium-throughput *C. elegans* growth data. PLoS One 4(9):e7018, PMID: 19753303, https://doi.org/10.1371/journal.pone.0007018.

Stenrød M, Klemsdal SS, Norli HR, Eklo OM. 2013. Effects of picoxystrobin and 4-n-nonylphenol on soil microbial community structure and respiration activity. PLoS One 8(6):e66989, PMID: 23818971, https://doi.org/10.1371/journal.pone.0066989.

Sun N, Youle RJ, Finkel T. 2016. The mitochondrial basis of aging. Mol Cell 61(5):654–666, PMID: 26942670, https://doi.org/10.1016/j.molcel.2016.01.028.

Sun N, Yun J, Liu J, Malide D, Liu C, Rovira II, et al. 2015. Measuring in vivo mitophagy. Mol Cell 60(4):685–696, PMID: 26549682, https://doi.org/10.1016/j.molcel.2015.10.009.

Tice RR, Austin CP, Kavlock RJ, Bucher JR. 2013. Improving the human hazard characterization of chemicals: a Tox21 update. Environ Health Perspect 121(7):756–765, PMID: 23603828, https://doi.org/10.1289/ehp.1205784.

Todorovic M, Wood SA, Mellick GD. 2016. Nrf2: A modulator of Parkinson's disease? J Neural Transm (Vienna) 123(6):611–619, PMID: 27145762, https://doi.org/10.1007/s00702-016-1563-0.

Uttley N. 2011. Product profile: picoxystrobin. http://www.agribusinessglobal.com/agrichemicals/fungicides/product-profile-picoxystrobin/ [accessed 15 February 2017].

Villeneuve C, Guilbeau-Frugier C, Sicard P, Lairez O, Ordener C, Duparc T, et al. 2013. p53-PGC-1α pathway mediates oxidative mitochondrial damage and cardiomyocyte necrosis induced by monoamine oxidase-A upregulation: role in chronic left ventricular dysfunction in mice. Antioxid Redox Signal 18(1):5–18, PMID: 22738191, https://doi.org/10.1089/ars.2011.4373.

Wallace KB, Eells JT, Madeira VM, Cortopassi G, Jones DP. 1997. Mitochondria-mediated cell injury. Symposium overview. Fundam Appl Toxicol 38(1):23–37, PMID: 9268603.

Wang Y, Huang R. 2016. Correction of microplate data from high-throughput screening. Methods Mol Biol 1473:123–134, PMID: 27518630, https://doi.org/10.1007/978-1-4939-6346-1_13.

Wang Y, Jadhav A, Southal N, Huang R, Nguyen D-T. 2010. A grid algorithm for high throughput fitting of dose-response curve data. Curr Chem Genomics 4:57–66, PMID: 21331310, https://doi.org/10.2174/1875397301004010057.

Weng Z, Luo Y, Yang X, Greenhaw JJ, Li H, Xie L, et al. 2015. Regorafenib impairs mitochondrial functions, activates AMP-activated protein kinase, induces autophagy, and causes rat hepatocyte necrosis. Toxicology 327:10–21, PMID: 25445804, https://doi.org/10.1016/j.tox.2014.11.002.

Weng Z, Zhou P, Salminen WF, Yang X, Harrill AH, Cao Z, et al. 2014. Green tea epigallocatechin gallate binds to and inhibits respiratory complexes in swelling but not normal rat hepatic mitochondria. Biochem Biophys Res Commun 443(3):1097–1104, https://doi.org/10.1016/j.bbrc.2013.12.110.

Williams PL, Dusenbery DB. 1988. Using the nematode *Caenorhabditis elegans* to predict mammalian acute lethality to metallic salts. Toxicol Ind Health 4(4):469–478, PMID: 3188044, https://doi.org/10.1177/074823378800400406.

Winklhofer KF, Haass C. 2010. Mitochondrial dysfunction in Parkinson's disease. Biochim Biophys Acta 1802(1):29–44, PMID: 19733240, https://doi.org/10.1016/j.bbadis.2009.08.013.

Zamzami N, Marchetti P, Castedo M, Hirsch T, Susin SA, Masse B, et al. 1996. Inhibitors of permeability transition interfere with the disruption of the mitochondrial transmembrane potential during apoptosis. FEBS Lett 384(1):53–57, PMID: 8797802.

Zheng X, Hunter T. 2013. Parkin mitochondrial translocation is achieved through a novel catalytic activity coupled mechanism. Cell Res 23(7):886–897, PMID: 23670163, https://doi.org/10.1038/cr.2013.66.